2.05 Radiation Effects in UO_2[☆]

Thierry Wiss, Alessandro Benedetti, and Emanuele De Bona, European Commission, Joint Research Centre, Karlsruhe, Germany

2.05.1	**Introductory Remarks**	125
2.05.2	**The Slowing Down of Energetic Projectiles in UO_2**	126
2.05.2.1	Main Processes	126
2.05.2.1.1	Nuclear energy losses (S_n)	126
2.05.2.1.2	Electronic energy losses (S_e)	127
2.05.2.1.3	Synergetic effect of electronic and nuclear energy deposition	129
2.05.2.2	Main Damage Sources	130
2.05.2.2.1	Energy loss and displacements produced by neutrons	130
2.05.2.2.2	Energy loss and displacements produced by (β,γ)-decays	131
2.05.2.2.3	Energy loss and displacements produced by α-decays	131
2.05.2.2.4	Impact of fission fragments	132
2.05.3	**Range of Different Projectiles in UO_2**	134
2.05.3.1	Basic Effects of Radiation Damage	134
2.05.3.2	Point Defects Formation	135
2.05.3.3	Modeling of Point Defects	136
2.05.3.4	Extended Defects	137
2.05.3.4.1	Dislocation loops	137
2.05.3.4.2	Prismatic loops	138
2.05.3.4.3	Void nucleation and growth	138
2.05.4	**Radiation Effects in UO_2 and in UO_2 Based Fuels**	139
2.05.4.1	Change in Chemical Properties	139
2.05.4.2	Change in Bulk Physical Properties	140
2.05.4.3	Elastic Properties	141
2.05.4.4	The High Burnup Structure	141
2.05.4.5	Can Polarons Explain the Radiation Resistance of UO_2?	145
2.05.5	**Conclusions and Perspectives**	146
References		146

Nomenclature

dpa Displacements per atom
FBR Fast breeder reactor
FPs Fission products
GB Grain boundary
HFP Heavy fission product
HBS High Burnup Structure
HZE High (H) atomic number (Z) and energy (E)
LFP Light fission product
LWR Light water reactor
MD Molecular dynamic
pka Primary knock-on atom
S_e Electronic energy losses
SEM Scanning electron microscope
S_n Nuclear energy losses
SRIM Stopping and range of ions in matter
TEM Transmission electron microscope

2.05.1 Introductory Remarks

The macroscopic, observable, and often technologically crucial results of exposure of solids to energetic particles are collectively known as *radiation effects*. The primary microscopic events that precede the appearance of gross changes in the solid are called *radiation damage*. This branch of the physics attempts to predict not only the number and the configuration of the point defects

[☆]*Change History*: December 2019. Thierry Wiss, Alessandro Benedetti, and Emanuele De Bona has updated the text and references.
This is an update of Wiss, T., 2012. Chapter 2.18 – Radiation Effects in UO_2. In: Konings, R.J.M. (Ed.), Comprehensive Nuclear Materials, Elsevier. pp. 465–480.

(vacancies and interstitial atoms) produced by the bombarding particles but also their evolution toward extended defects resulting from their coalescence.

UO_2 is today's most commonly used fuel material in nuclear power reactors. Nuclear fuels have to operate safely for years under severe conditions of radiation damage. Heat production from the nuclear fuel in order to generate electricity ensues mostly from the slowdown of the fission products (FPs) that is high-energy heavy ions but also from their further radioactive decay most frequently by γ- or β-decay. The heat dissipated in the lattice of the crystalline material constituting the conventional nuclear fuels is a primary effect from the energy losses of the fission fragments by nuclear or electronic interactions on the atoms constituting the fuel. As a direct consequence, there are also defects created along the path of the fission fragments leading to modification of the physical properties of the fuel.

In addition to the fission process, damage is also created by α-decay, particularly in the fuels containing strong alpha-emitters (minor actinides), but also from β- and γ-decay from FPs.

In this article, basic processes of energy losses are given and stopping power and range of various ion/particles defined for the specific case of UO_2. The radiation damage produced by the passage of these ions/particles is conceptually described.

The impact of defect creation on the physicochemical properties of UO_2 is then be described with particular emphasis on its use as nuclear fuel. Fuel operating conditions are taken into account in addition to concomitant effects of damage sources when discussing the overall behavior of UO_2 during irradiation and also during (long-term) storage.

Uranium dioxide has been extensively studied, and an exhaustive list of publications related to the radiation effects is impossible. The reader is referred to more detailed publications covering UO_2 properties by Belle,[1] radiation damage processes in UO_2 by Lemaignan[2] or processes of damage in nuclear fuel by Olander,[3] for example.

The physical processes of radiation damage had started soon after the discovery of radioactivity by Henri Becquerel in 1896. There was very soon interest in how particles from radioactive decay were slowed down in matter. Marie Curie has stated, "les rayons alpha sont des projectiles susceptibles de perdre de leur vitesse en traversant la matière" (α rays might lose part of their speed while traveling through matter).[4] Thomson, Bohr and Rutherford were pioneers in studying the effect of particles interactions with matter.[5,6,7,8] The development of ion accelerators allowed extensive studies on radiation damage in all types of materials. Linked to the use of the Monte Carlo code stopping and range of ions in matter (SRIM) for the estimation of energy loss, range, and damage, the description of the main processes of particles/ions interactions with matter is given.[9] The investigation of irradiated fuel being more difficult, numerous studies were performed on ion-irradiated UO_2 in order to understand the basic mechanisms of damage evolution.

2.05.2 The Slowing Down of Energetic Projectiles in UO_2

In the context of physical processes occurring in nuclear fuels involving energy dissipation, all type of radiations should be considered. When the conditions are met for a fission to occur, about 200 MeV energy is dissipated in the fuel lattice. Most of this high energy is carried by FPs, with masses ranging from 75 to 160, that is, elements between Ga and Dy. The FPs fall into two groups: the light ones, typically Kr, with about 100 MeV energy, and the heavy ones, typically Ba, with about 70 MeV energy. Intense neutron fluxes, produced by the fission reactions themselves, with energies ranging from eV to MeV are necessary to sustain the controlled nuclear chain reaction. An intense ß-, γ-radiation field is also present because most FPs are radioactive with different decay energies and very different half-lives. Additionally, α-decay occurs from the original actinides, and even more so, from large amounts of "minor actinides," e.g., Np, Am, and Cm that are formed by successive neutron capture during the operation of the fuel. The α-decay has to be accounted for not only during reactor irradiation (at elevated temperature), but also during storage before and after reactor irradiation, that is under conditions where thermally activated damage recovery is largely or fully absent.

In terms of energy releases, two major processes have to be considered, that is inelastic collisions and ballistic (elastic) collisions depending on the type of projectile and its physical characteristics such as energy and mass. In given conditions, both processes can occur simultaneously in different proportions. The next paragraphs summarize these aspects with particular emphasis on the UO_2 nuclear fuel.

2.05.2.1 Main Processes

Energetic charged particles interact independently with the nuclei and the electrons in a solid. Basically, the energy loss of a charge particle can occur through four different processes:

(1) Inelastic collisions with an electron (main process of energy loss producing excitation and ionization).
(2) Inelastic collisions with a nucleus (Bremsstrahlung and coulumbic excitation).
(3) Elastic collisions with a nucleus (Rutherford diffusion).
(4) Elastic collisions with an electron.

2.05.2.1.1 Nuclear energy losses (S_n)

When the energy of a given particle/ion is sufficiently low, elastic collisions with nuclei occur. The main process, called Rutherford diffusion is the result of the transfer of kinetic energy from the impinging particle/ion to a target atom. The resulting effects

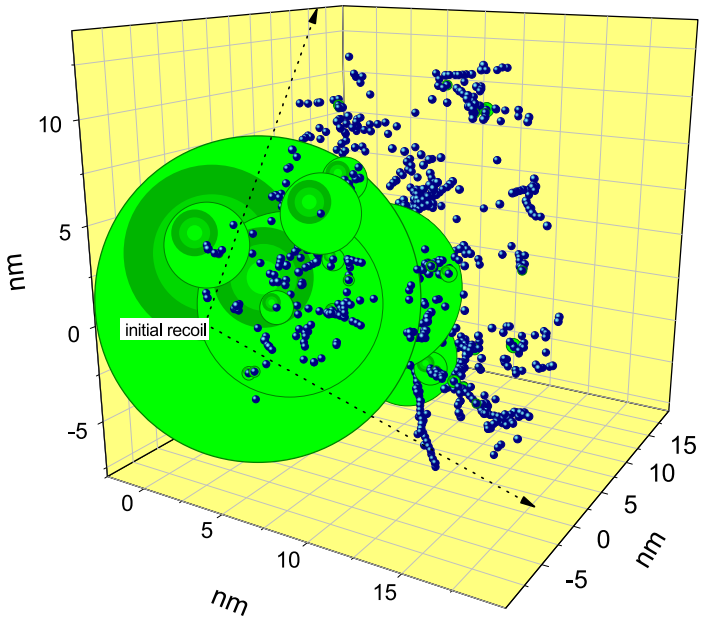

Fig. 1 Collision cascade produced by a recoil nucleus during an α-decay (the energy is typically 100 keV). The cascade has been calculated with SRIM2003. Reproduced from Ziegler, J.F., Biersack, J.P., Littmark, U., 1985. The Stopping and Range of Ions in Solids. Pergamon Press Oxford. With permission of the European communities. © European Atomic Energy Community.

(described more extensively in the next paragraphs) are the displacements of atoms from their regular lattice site. If such a knock-on atom has gained sufficient kinetic energy from the collision it can itself generate a new collision, hence a displacement. The energy necessary to displace an atom from its lattice site is called displacement energy and its values in UO_2 ranges from 20 to 40 eV for oxygen and uranium atoms, respectively.[10] If the total energy from an incident particle is high enough, repeated collision-displacement sequences produce collision cascades. **Fig. 1** shows such a collision cascade produced by a recoil nucleus during an α-decay (the energy is typically 100 keV). The cascade has been calculated with SRIM2003.[9] The "size" of the knock-on atoms represents the energy transferred during the collisions. The green spheres are uranium and the blue spheres oxygen. In a collision cascade, the typical energy transferred is 50 eV but some collisions with a large cross-section can produce energy transfer of a few kiloelectron volt, which explains the formation of sub-cascades. The resulting displaced atoms either recombine or leave permanent defects, which is discussed in another section.

For a more recent study of the thermal history of a displacement cascade see Martin *et al.*,[11] from whose work **Fig. 2** is taken. It pictures an MD simulation of a 10 keV cascade between two parallel planes, after 0.35 ps and at 700K, when the disordered volume V is maximum.

2.05.2.1.2 Electronic energy losses (S_e)

Electronic energy losses and their effects have been extensively described. Different concepts have been proposed to explain the formation of ion tracks in matter by the slowing down of swift heavy ions in the electronic stopping power regime. The "ionic spike" model for insulators of Fleischer *et al.*[12] assumes a high ionization rate of the lattice-atoms surrounding the path of the incoming ion, which leads to a local explosion due to high Coulomb repulsions. However, it has been shown that the electronic stopping power threshold deduced from the etching of several insulators cannot be scaled by using the parameters governing this model, but can be rather related to the thermal conductivity of the material. This leads many authors to reconsider the thermal-spike model. The basic assumption in the thermal-spike model originally proposed by Seitz and Koehler[13] is that around the trajectory of the high-energy ion a high-temperature region is formed in the material. The maximum temperature reached in a cylinder around the ion trajectory may surpass the melting point T of the material, as, e.g., in UO_2 (with T = 3150K). In a model revisited by Toulemonde *et al.*,[14] thermodynamic parameters of UO_2 have been taken into account to calculate the radius of observed ion tracks in UO_2. This model takes into account that energetic ions transfer their energy in a first step to the target electrons and then to the lattice via electron–phonon interactions leading to a heating of the lattice. It is assumed that the effect of the electron–phonon coupling can be described by the parameter λ, the mean diffusion length of the energy deposited on the electrons.

This parameter is linked to the electron–phonon coupling constant, g, by the relation $\lambda^2 = D_e \tau_a$ where $\tau_a = C_e/g$ is the mean electron–phonon interaction time, C_e is the specific heat of the electrons (($D_e \sim 2$ cm^2 s^{-1} and $C_e \sim 1$ J cm^{-3} K^{-1})), and D the electron diffusivity. As suggested by Baranov *et al.*,[15] we shall consider these values of C_e and D_e to be constant, since the hot electrons in the conduction band of an insulator will present the same behavior as in metals. Using different values of λ as a variable parameter, the track radius was calculated as a function of (dE/dx). For a value of $\lambda = 6$ nm, **Fig. 3** shows the calculated

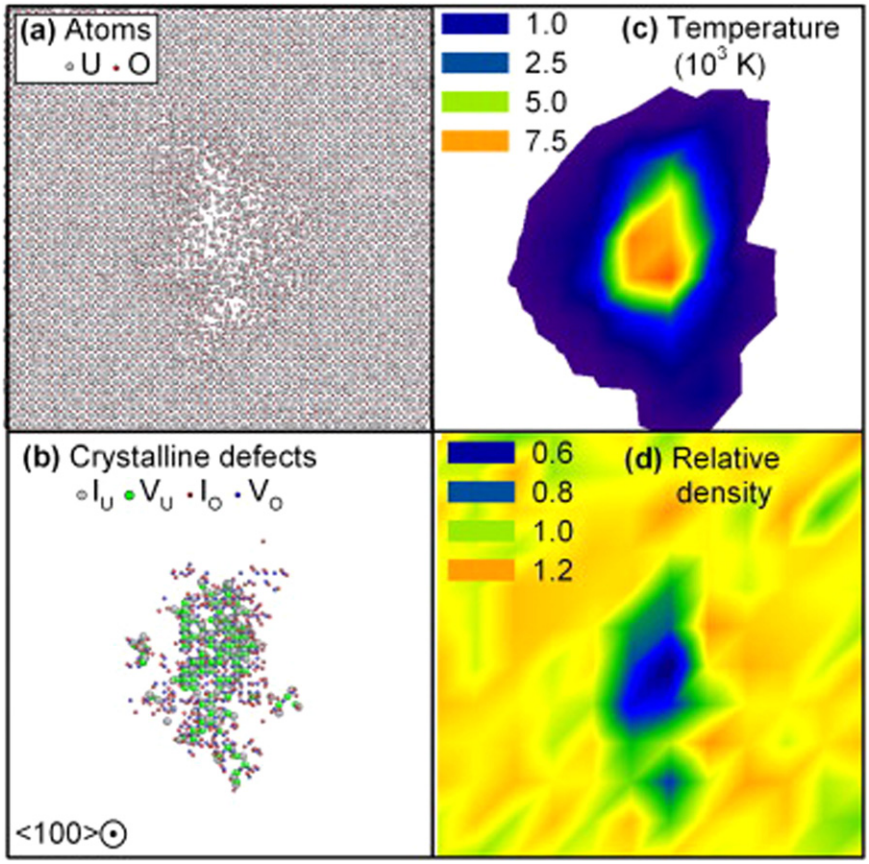

Fig. 2 MD simulation of a 10 keV cascade initiated at 700K shown between two appropriate planes after 0.35 ps: atoms (a), crystalline defects (b), local temperature (c) and local density relatively to UO_2 density (ρ at 700K) (d). From Martin, G., *et al.*, 2014. A thermal modeling of displacement cascades in uranium dioxide. Nucl. Instrum. Methods Phys. Res. Sect. B: Beam Interact. Mater. At. 327, 108–112.

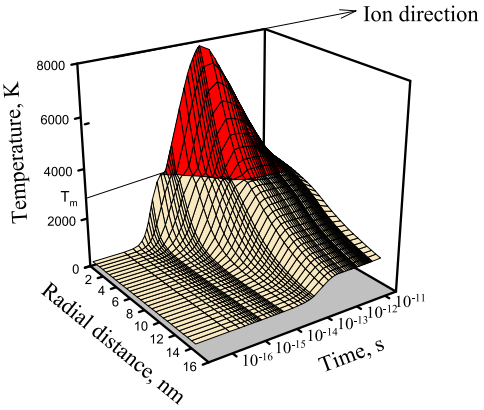

Fig. 3 Calculated evolution of the UO_2 radial temperature distribution along a track in UO_2 as a function of time. The calculations are for 11.4 MeV/u U ions in the first nm of the target, that is, dE/dx = 60 keV/nm with λ = 6 nm and a melting temperature of T_f = 3150K. Reproduced from Wiss, T., *et al.*, 1997. Swift heavy ion damage in UO_2. Nucl. Instrum. Methods Phys. Res. B, 122, 583.

lattice temperature as a function of time and radial distance from the ion path for a 11.4 MeV/u U ion in UO_2. The peak temperature of the spike increases to its maximum value within a very short time, about 10^{-13} s, then it decreases and the spike broadens as a result of heat conduction.[16] A similar calculation for 173 MeV Xe ions with (dE/dx) = 29.1 keV/nm also shows a good correlation between measured and calculated track radii, demonstrating, at least for the few values of dE/dx studied here, that this model can be successfully applied to UO_2. The present results add, thus, further evidence to the existence of thermal-spike

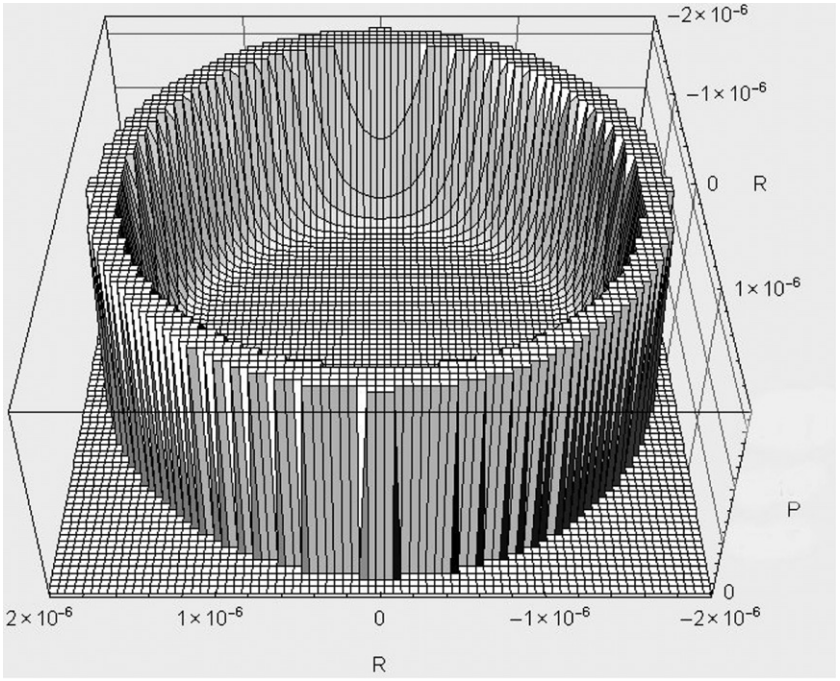

Fig. 4 Pressure wave calculated 10 ps after passage of a fission fragment. The mesh (0.5 nm) is close to the uranium interdistance in the UO_2 lattice. The unit pressure P is 10^4 N cm^{-2}. R is given in cm. With permission of the European communities. © European Atomic Energy Community.

effects produced by fission fragments in UO_2. Previous evidence included: (1) Transmission Electron Microscopy (TEM) observations of a fission-spike induced phase change in U_4O_9 needles present in UO_{2+x} (this transformation occurs at T = 1150°C),[17] (2) fission-enhanced diffusion of U in UO_2, which can only be explained by thermal and pressure effects of fission spikes[18] and (3) evidence of fission gas resolution (destruction of fission gas bubbles) due to the passage of FPs.[19]

More recently, Ishikawa *et al.*[20] investigated the ion-track size in CeO_2 and UO_2 irradiated with ions with energy in the order of 1 MeV/u and reported a smaller ion-track size for the latter, despite the two materials having the same crystallographic structure and similar thermal properties.

A possible explanation was given by Weber,[21] who attributed it to the fact that thermal recovery of α-induced lattice parameter variations is more pronounced in UO_2 than in CeO_2, therefore indicating that radiation damage in UO_2 is relatively unstable and in turn suggesting that recrystallization of UO_2 may be easier than that of CeO_2.

In another model, the formation of ion track in UO_2 has been described by the propagation of a pressure wave created along the path of an energetic fission fragment under specific geometrical conditions. It is shown that a large fraction of the fission fragment electronic losses is converted in strong shock waves whose passage in the solid is too fast for producing atomic displacements, but which can nevertheless release high amount of energy by transferring it to the surface of the fuel pellet. The consequent matter displacements have been shown to have important effects on the structural properties of the nuclear fuel. Surface tracks could be explained by the expulsion of material when this pressure wave reaches the surface.[22]

Non-linear heat transport models were examined to explain the conversion of the fission fragment energy into thermal and mechanical energy in times less than a few picoseconds.

Fig. 4 shows the shock wave pressure generated by a fission fragment with 18 keV nm^{-1} energy loss after 10 ps. The chosen core radius of 10 nm produces a temperature (3030K) close to the UO_2 melting point and after 10 ps the pressure wave has propagated 200 nm in radius and has decayed from 9.5×10^{10} to 10^9 dyn cm^{-2}. More details can be found in Ref. 22.

As an example of the effect of fission spikes, the porosity of sintered UO_2 pellets, which controls the thermal and mechanical performance of a fuel rod, is gradually destroyed by fission tracks through a fuel densification process known in reactor technology as "in-pile sintering." This effect, inexplicable in terms of customary matter diffusion, is strictly related to long-range distortions caused by surface tracks. Fig. 5 shows a TEM micrograph of an LWR UO_2 fuel irradiated at 35,000 MWd/t. The dotted white area indicates the location of an initial sintering pore where radiation enhanced re-densification (in-pile sintering) occurred through the passage of fission fragments.

2.05.2.1.3 Synergetic effect of electronic and nuclear energy deposition

Ion implantations are typically used for single effect studies to assess the behavior of UO_2 against damage formation. In multiple irradiation, depending on the sequence between different ions with different properties, (e.g., energy loss) or even simultaneity of irradiations the effects can vary substantially. The synergetic effect of irradiation in the two energy loss regimes (nuclear, electronic) (SNEEL) has been described in 2015 by Thomé *et al.*[23] for the case of SiC. More recently Gutierrez *et al.* performed a study on the

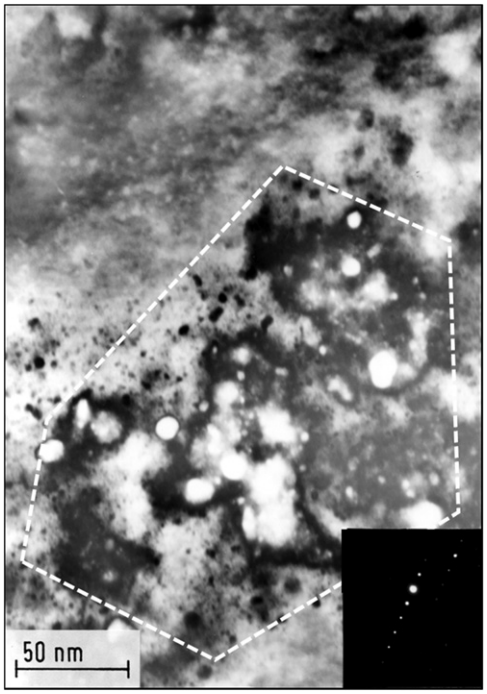

Fig. 5 TEM micrograph of an LWR UO_2 fuel irradiated at 35,000 MWd/t. The dotted white area indicates the location of an initial sintering pore re-filled with UO_2 through fission spikes. With permission of the European communities. © European Atomic Energy Community.

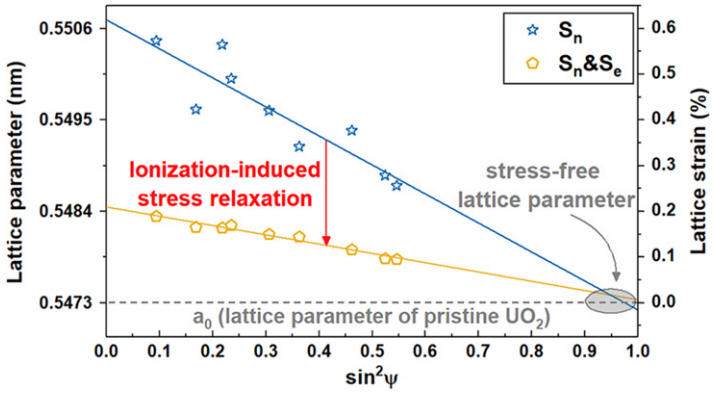

Fig. 6 Lattice parameter as a function of the crystallographic-planes inclination angle ($Sin^2\Psi$-method) of irradiated, polycrystalline UO_2. From Anderoglu, O., 2005. Residual Stress Measurement Using X-Ray Diffraction. Texas A & M University. Gutierrez, G., *et al.*, 2019. Effect of coupled electronic and nuclear energy deposition on strain and stress levels in UO_2. J. Nucl. Mater. 519, 52–56.

synergetic effect on the irradiation response of UO_2,[24] in which they found that strain and stress levels in a UO_2 polycrystalline sample irradiated in both the Sn and the Se regimes (that is, simultaneously with two ion beams) were lower when compared to irradiation performed in Sn alone. This result is a direct evidence of a coupled effect of nuclear and electronic energy deposition in UO_2. It proves that ionization can modify the characteristics, in terms of both defect structure and density, of the defects generated by nuclear collisions. In addition, it is shown that the thin irradiated layers maintain, in the plane of the samples, the lattice parameter of the pristine UO_2 bulk crystal as shown in Fig. 6. These results should provide new insights on the in-pile behavior of the nuclear fuel.

2.05.2.2 Main Damage Sources

2.05.2.2.1 Energy loss and displacements produced by neutrons

In nuclear reactors, three types of neutrons are considered: the thermal neutrons with energy $E < 1$ eV (0.025 eV), the epithermal neutrons with, 1 eV $< E <$ 10 keV and the fast ones with $E >$ 10 keV. In the energy domain typical of fission produced neutrons, only elastic collisions and capture are considered. In most reactors, the energy loss by the neutrons in the moderator is the *sine qua*

non condition for a controlled fission reaction chain to occur while the remaining fast neutrons (not thermalized) only create damage in the fuel and on the structure materials.

A neutron of mass $m = 1$ and of energy E_n, while passing through a medium of mass M_1, will occasionally collide (mean free path $\sim$ 1 cm) with a lattice atom, imparting to it an energy (depending on the impact parameters) up to a maximum value given by

$$E_{\max} = \frac{4mM_1}{(m+M_1)^2}E_n \qquad \text{or} \qquad \sim \frac{4E_n}{M_1} \qquad \text{for } M_1 \gg m$$

The *maximum* pka (primary knock-on atom) energy for a neutron of energy $E_n = 1$ MeV in UO_2 is, therefore, 17 keV for U, and 250 keV for O, respectively; however, most interactions with neutrons will lead to a smaller energy transfer.

The *minimum* neutron energy to produce one displacement is given by $E_{min} = E_d$, where E_d is the displacement energy (for example, 20 eV for O and 40 eV for U in UO_2).[7] Hence

$$E_n^{\min} \sim 0.1 \text{ kev}$$

Thermal (low energy) neutrons thus do not produce direct displacements. On the other hand, primary knocked-out atoms may in turn knock out other atoms, inducing a cascade effect in the lattice.

2.05.2.2.2 Energy loss and displacements produced by (β,γ)-decays

For β-decays of the FPs in nuclear fuels the energy distribution is a continuum with $E_{\beta max}$ (typically 2.6 keV $< E <$ 10.4 MeV). The e^- and e^+ produce ionization and excitation along their path and the nuclear scattering is very large. Rutherford scattering cross-section is proportional to $(M_1/m_0)^2$ and the cross-section ratio $\sigma_{e-}/\sigma_{p+} = 4\ 10^6$. In fact σ can be extremely large and target e^- have to be considered.

Electrons can also produce isolated displaced atoms if their energy is high enough. The minimum energy, $E_e^{\min}$, to displace a lattice atom is given by

$$E_d = 2\frac{m_0}{M}\frac{E_e^{\min}}{m_0c^2}\left(E_n^{\min} + 2m_0c^2\right)$$

where m_0 is the electron mass, M the mass of the displaced atom and c the velocity of light. β-decay causes thus very few, isolated point defects.

The emission of photons, γ but also X-rays in nuclear fuel will be neglected in this section. Heating effects and ionization also take place, but their consequences compared to the other damage sources during operation of nuclear fuel, for example, are negligible.

2.05.2.2.3 Energy loss and displacements produced by α-decays

A heavy recoil atom, e.g., Np^{237} in the decay of Am^{241}, receives a recoil energy E due to conservation of momentum, $ME = mE_\alpha$, hence typically $\sim$ 100 keV (91 keV in the decay of Am^{241}). These recoil atoms show predominantly nuclear stopping and produce a dense collision cascade with typically $\sim$ 1500 displacements within a short distance of $\sim$ 20 nm. Defect clustering can occur, stabilizing the damage.

In general, ions passing through matter lose energy via two processes, either by direct collisions with the atoms of the matter (elastic collisions) or by dissipating their energy on the electrons (inelastic collisions), hence nuclear energy loss $(dE/dx)_n$ leading directly to displaced atoms, or ionizations (electronic energy loss $(dE/dx)_e$). **Fig. 7** shows the particular case of an α-decay that evidences that the heavy recoil nucleus loses its energy mainly via nuclear energy losses whereas the light α-particle does mainly by electronic energy losses. Any given radiation source can suffer these two types of energy loss. The case of α-decay in UO_2 is partially included in **Fig. 1** showing a displacement cascade produced by the recoil atom of the decay of U^{238}, that is ^{234}Th, and schematized in **Fig. 7**.

Fig. 9 shows the energy loss of the α-particle which is predominantly electronic by comparison with the recoil nucleus (see also **Table 1**: Displacements induced in UO_2 by different damaging sources).

The effects of α-damage in UO_2 have been studied for decades, either by external irradiations with α-particles or heavy ions simulating the recoil nucleus,[25] or by doping UO_2 with strong α-emitters (e.g., ^{238}Pu).[21,26,27] The formation of point defects and

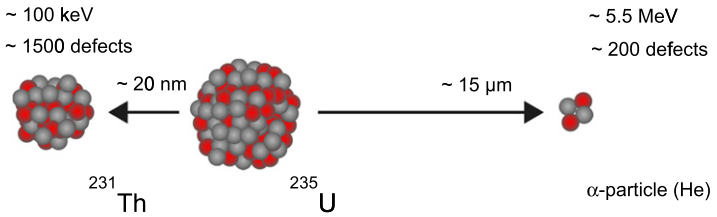

Fig. 7 Scheme of an α-decay event in UO_2. About 100 keV of energy is dissipated by the recoil nucleus mainly elastically, whereas about 5.5 MeV are lost mainly inelastically by the α-particle, until it comes to rest and become a helium atom. With permission of the European communities. © European Atomic Energy Community.

Table 1 Displacements induced in UO_2 by different damaging sources

	Energy, keV	*Range, μm*	*Fraction of energy lost by elastic (nuclear)/inelastic collisions (electronic)*	*Number of defects formed, N*
Light fission product	~95,000	9	0.03/0.97	40,000
Heavy fission product	~70,000	7	0.06/0.94	60,000
α–particle	5500	15	0.01/0.99	200
Recoil atom	95	0.02	0.90/0.10	1500

Source: © European Atomic Energy Community.

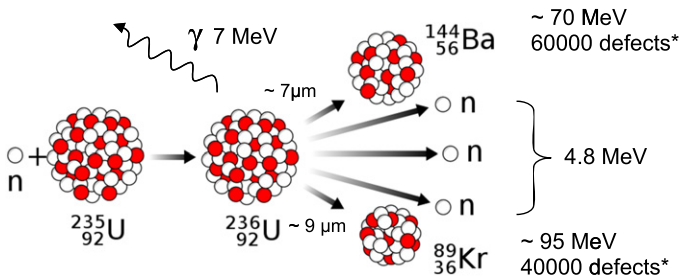

Fig. 8 Scheme of a fission event. About 200 MeV of energy are dissipated by the fission of a ^{235}U nucleus in kinetic energy of the fission fragments, neutrons, γ-rays and UO_2 lattice heating. The defects produced by the fissions fragments have been calculated using SRIM2008 and represent only ballistic effects. With permission of the European communities. © European Atomic Energy Community.

their evolution into extended defects, but also the consequences on the UO_2 lattice (e.g., lattice swelling) and on the modification of its thermo-physical properties, have been assessed.[28] The studies on α-damage also aim at determining the long term evolution of spent nuclear fuel during storage and more specifically what to expect in terms of integrity or behavior against corrosion if in contact with water.[29–31] Moreover α-decay in spent nuclear fuels can provoke a number of negative effects in the long term: fuel matrix swelling, embrittlement, gas release and increased fuel sheath stress.[32] The specific aspects of α-damage on the behavior of spent fuel are reported in another article.

2.05.2.2.4 Impact of fission fragments

Fission produces two FPs as well as 2–3 neutrons. As mentioned in Section 2.05.1, FPs fall into two groups, the light ones (LFPs) and the heavy ones (HFPs). Further typical values (for the case of UO_2) are given in **Table 1** and in **Fig. 8** below. The exact values depend on the physical parameters of the material (e.g., displacement energy, E_d, atomic number, density etc.). Because of the high energy deposition rate, typically 20–30 keV/nm, a locally (over-) heated track (either a fission spike or a thermal spike) may be formed. In general, thermal spikes, deriving from high energy collisions of the fission fragments with the medium dissipate heat from the electronic type energy losses but generate less visible defects. Experimental evidence supports this view: in irradiated UO_2 samples, point defect clusters are only found along secondary, less energetic recoils, whereas no evidence is seen along the fission fragment path.

However, for an irradiated material most damage occurs at its physical boundaries, where creation of surface defects (from Schottky point defects to macroscopic extended defects) results in bulk swelling or densification processes. Material displacements, called surface tracks, appear thus at the points of emergence of fission fragments. These defects affect in different ways the geometrical stability of the nuclear fuel. As an example, the porosity of sintered UO_2 pellets, which controls the thermal and mechanical performance of a fuel rod, is gradually destroyed by fission tracks through a fuel densification process known in reactor technology as "in-pile sintering" as shown in **Fig. 5**. This effect, inexplicable in terms of customary matter diffusion, is strictly related to long-range distortions caused by surface tracks.

These fission tracks are observable in TEM images, since they cause a distortion of the lattice, and therefore give rise to diffraction contrast, in most materials. A thorough analysis of fission tracks formation in UO_2 was presented by Ronchi *et al.*[22]

Most of the energy is transferred by electronic energy loss, in particular for the more energetic light FPs. This, in addition to causing local heating up to or above the melting point, can cause formation of additional defects and/or rearrangement of existing defects. An extreme case is the destruction of pre-existing fission gas bubbles by the passage of a fission spike, known to occur in the conventional nuclear fuel, UO_2.[33]

However, more recently, molecular dynamics was employed by Huang *et al.*[34] in order to simulate the behavior of Xe bubbles in UO_2; they concluded that bubble re-solution due to the electronic stopping of fission fragments in UO_2 is negligible with respect to homogeneous re-solution.

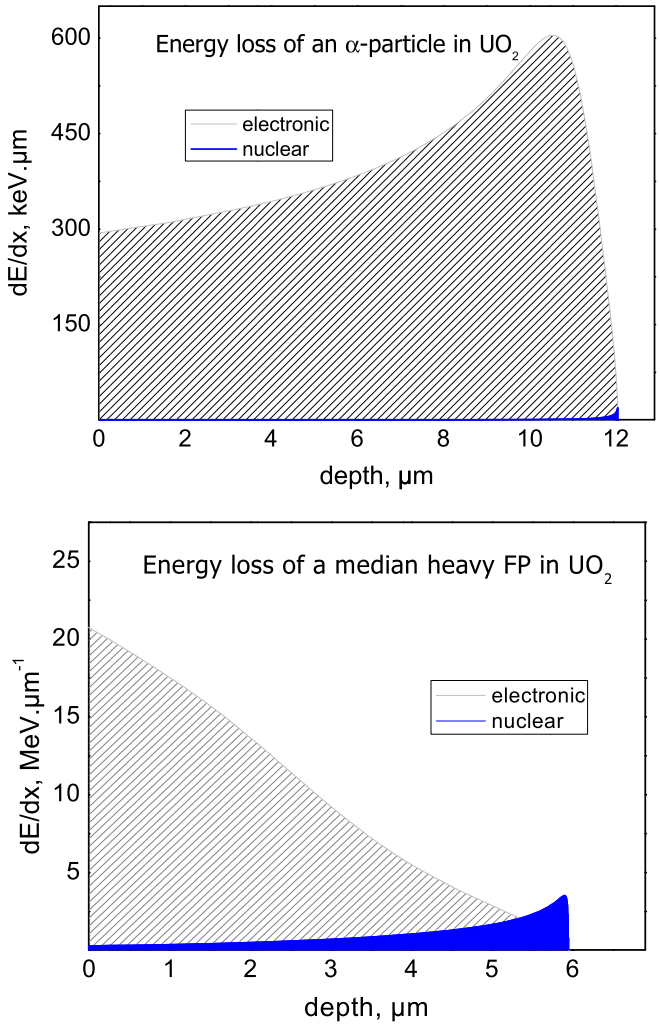

Fig. 9 Electronic energy loss (dashed lines) and nuclear energy losses (black area) of a typical α-particle (upper part) and of a median fission product (lower part) in UO_2. With permission of the European communities. © European Atomic Energy Community.

The following is a short description of the sequence of events in the fission spike:

(1) Primary phase or ballistic phase – the passage of the fission fragment – is very short but it defines the initial size and shape of the spike. Most Frenkel defects are produced by secondary collision cascades. The deposited Coulomb energy is dissipated into local heating through electronic interactions with recoiling ions to produce a thermal spike.
(2) Secondary or quenching phase – recombination of vacancies and interstitials occurs when the spike comes to thermal equilibrium. An interstitial-rich outer zone and a vacancy-rich inner zone form. The hydrostatic pressure field originally created by the molten core of the spike – contributing to the separation of the interstitials from the vacancies of the Frenkel pairs formed in the primary phase – is replaced by compressive stresses in the outer zone and tensile stresses in the core.
(3) Third or track annealing phase – more recombination occurs, and some vacancy clusters are stabilized by fission gases forming embryos for later bubbles.

The processes in these three phases are repeated many times all through the fuel volume in a homogeneous material. The whole fuel is affected after a rather short time, the level of one displacement per atom, dpa, being typically reached within <1 day. This value is certainly an underestimation, as it does not account for the displacement caused by electronic energy losses (thermal spike causing pressure waves).[22]

The consequences are significant fission-enhanced diffusion, fission-enhanced creep, re-solution of fission gas from bubbles, etc.

Fig. 9 shows the large difference in electronic energy loss, $(dE/dx)_e$, between the α-particles and the fission fragments. The energy loss curves show the electronic and nuclear stopping that is the ionization part, with high values (18–22 keV/nm) at the point of fission (full ion energy) for the case shown, that is UO_2. The nuclear stopping, that is the displacement damage part, peaks

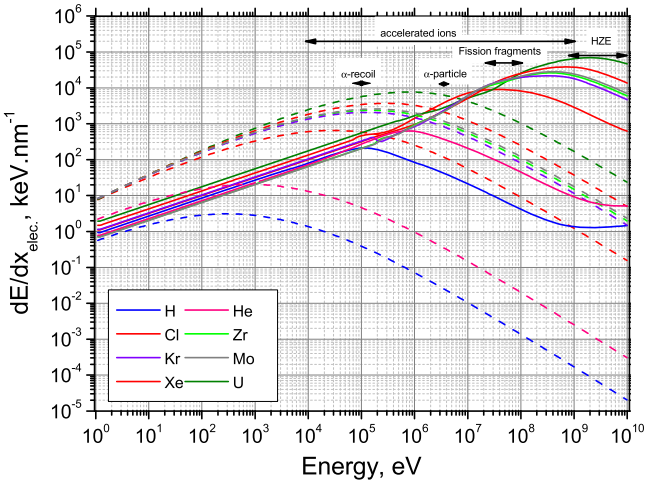

Fig. 10 Electronic energy loss (dashed lines) of various ions in UO_2. With permission of the European communities. © European Atomic Energy Community.

at the end of the range ($\sim$ 1 keV nm^{-1}) and is very small (but still present) at the point of fission ($\sim$ 0.1 keV nm^{-1}). The ratio of nuclear to electronic stopping is always low for those high energies, but it varies between 1:180 at the fission site and about 1:3 toward the end of the range, to become even about 1:1 at the very end.

The recoil atoms of the α-decay and the high defect density produced by their slowing down are also included in the **Fig. 1**; the nuclear stopping power is obviously predominant but also shows a large difference in range (see **Fig. 7**): about 1500 displacements are formed along a very short track of only $\sim$ 20 nm.

It can also be seen as various ions produced in accelerators can reproduce energies involved in most type of decays including fissions (being spontaneous or neutron induced). For cosmic rays and High-Energy nuclei (HZE) it can be noted that almost their entire energy is dissipated inelastically as shown **Fig. 10**.

Fig. 10 shows the energy loss of a typical light fission fragment (for example Zr) as a function of its energy. In **Fig. 10**, the energy displayed covers a range beyond fission energy to show that when increasing the energy above a threshold corresponding to the coulombic barrier, the energy loss decreases. This is to contribute to the fact that the fission fragment is fully ionized and that when increasing energy the velocity also increases, reducing the energy transfer for a given unit length. Two energy losses can indeed correspond to two different ion energies.

The energy losses in UO_2 for different projectiles can result in the formation of defects in different proportions as a function of their nature. The ballistic effects can be easily converted into a certain number of instantaneous defects formed (although instantaneous recombinations are not easy to quantify). The electronic energy losses result generally in less quantifiable effects for a single projectile. The next paragraphs will give more insights on these phenomena.

2.05.3 Range of Different Projectiles in UO_2

Because of numerous collisions with energy transfer to the target atoms, a given ion or particle will have a defined trajectory with a given length. From the energy losses, either elastic or inelastic, the penetration range of a given particle can be predicted as shown **Fig. 11**. Whereas the high energetic particles/ions experience only few scattering events (due to the low cross-section for nuclear scattering), and hence are almost not deviating from their original direction, the low energy ones might experience high angle scattering.

As a function of the mass of the particle/ion, it can be noticed that the range decrease with increasing mass is directly correlated to the charge of the ions at a given energy. When the ions are fully ionized at certain energy, hence a given speed, the energy loss decreases and the range proportionally increases again. This phenomenon can be observed in **Fig. 11** for the heavier ions (Kr, Zr, Xe) showing an inflexion in their range above 100 MeV, corresponding to their nearly full ionization.

2.05.3.1 Basic Effects of Radiation Damage

During the slowing down of a particle/ion in a target, the history of the particle is represented by its energy loss, its range, and the interactions with the media it is passing through. As interactions one has to primarily consider the displacements, recombination, ionizations and excitations in order to assess the radiation damage build-up. Additionally, complexes can be formed between different kinds of point defects, e.g., point defects can rearrange and give origin to line defects.

In the following, we will focus on radiation damage in UO_2, as this material is by far the most common fuel in reactors and as such has been extensively investigated.

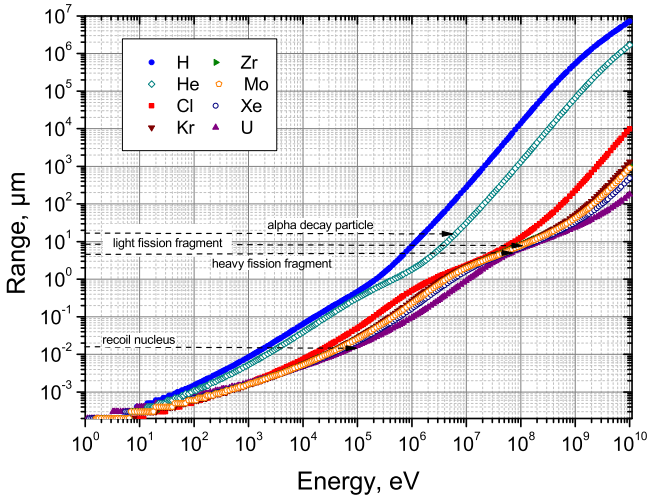

Fig. 11 Range in UO_2 of different projectiles as function of their energies. With permission of the European communities. © European Atomic Energy Community.

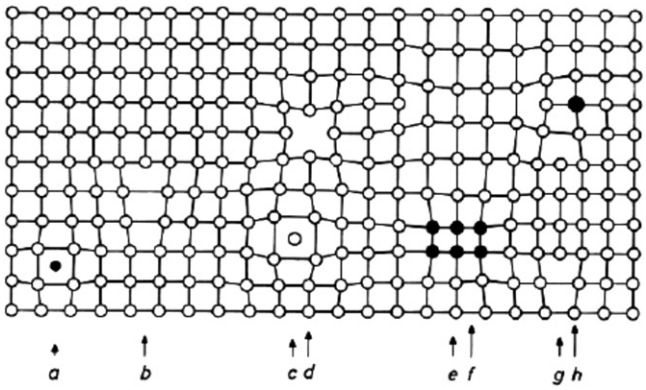

Fig. 12 Various crystal lattice defects: (a) interstitial impurity atom, (b) edge dislocation, (c) self-interstitial atom, (d) vacancy, (e) precipitate of impurity atoms, (f) vacancy-type dislocation loop, (g) interstitial-type dislocation loop, (h) substitutional impurity atom. With permission of the European communities. © European Atomic Energy Community.

2.05.3.2 Point Defects Formation

Unlike perfect lattices, all real crystals contain defects differentiated according to their dimension. The defects in a crystal can be triggered by the different kind of damage processes as described in the previous sections. The one-dimensional defect is called a point defect, implying that it involves only one atom surrounded by an otherwise perfect lattice. However, the presence of a point defect may affect the properties of its nearest neighbors, and, by way of elastic or electric interactions, a sizable spherical region of the lattice around the defect. Two types of point defects are intrinsic to the material, meaning that they form spontaneously in the lattice without any external intervention: the vacancy and the self-interstitial, shown schematically in Fig. 12 and referred as (d) and (c), respectively. The vacancy is simply an atom missing from a lattice site, which would be occupied in a perfect lattice.

The adjective "self" indicates that the interstitial atom is of the same type as the lattice atoms.

The defects referred as (a) and (h) in Fig. 12 show the two basic mechanisms by which a foreign or impurity atom can exist in the crystal lattice of a host element. In the latter case, large impurity atoms, usually of the same type as the host atoms (e.g., Pu in UO_2), replace the host atoms on regular lattice positions. These are called substitutional impurities. Although this can result in local lattice distortions, the structure of the lattice is not modified, except for the identity of the atoms occupying the lattice sites which is different. Small atoms that are chemically dissimilar from the host atoms may occupy interstitial positions and do not appreciably distort the surrounding host crystal (e.g., He in UO_2). They are termed interstitial impurities.

Self-interstitials and vacancies occur naturally in ionic crystals as well as in elemental solids.

However, because in UO_2 the cations (U) and anions (O) carry electrical charges ($+4$ and -2, respectively) vacancy and interstitial formation are not independent processes. To create a vacancy on the anion sublattice by moving the anion to the

surface, for example, would leave the surface negatively charged and the inner region around the vacancy with a net positive charge. This violation of local electrical neutrality prevents such a process.

The most stable charge states for the Fermi level in the middle of the band gap of almost all the defects in UO_2 are consistent with the ionic picture of this material. Charged states can therefore not be neglected, not only in the study of the defect formation but also in the investigation of their migration and of the migration of FPs.[35] Crocombette studied the variation of formation energies of point defects and clusters in UO_2 as a function of their charge states using density functional theory (DFT). Di- and trivacancies are considered as well as various assemblies of oxygen interstitials, namely, the cuboctahedral (either empty or filled) and the split-di-interstitial defects. The energies of formation of these defects for various possible charge states are calculated using the DFT + U approach. The energy gain upon clustering is vastly modified when the possible charge of defects is taken into account.[36]

Similar arguments apply to cation vacancies or self-interstitials of either ionic type. In UO_2, two anion vacancies need to be created for each cation vacancy, forming a Schottky trio. However, the dominant point defects in ideally pure stoichiometric UO_2 are anion Frenkel defects (defined as anions leaving their place in the lattice, creating a vacancy and becoming an interstitial by lodging in a nearby location), O^{2-} vacancies and O^{2-} interstitials.[37]

2.05.3.3 Modeling of Point Defects

Electronic structure calculations by ab initio techniques enable one to determine quantities inaccessible to experiments, either because of the scale being too small or the impossibility in isolating the contribution of a single factor to the physical properties. In particular, ab initio calculations allow to study of separately different types of point defects in a solid and to determine for each of them its stability (formation energy) or its influence on the crystal structure (local relaxation around the defect, swelling of the crystal). Many work contributed to assess the energy associated to these different defects in UO_2 as well as in non-stoichiometric UO_2: see, for example, Freyss *et al.*[38] and Yakub *et al.*,[39] who were able to describe the whole set of high-temperature properties of solid, hyperstoichiometric UO_{2+x}. More recently, Soulié *et al.*[40]confirmed that oxygen interstitials are dominant at high T, either in isolated form or in clusters depending on the deviation from stoichiometry, whereas below 1300 K they expect uranium vacancies to be prevail in the stoichiometric material. Cooper *et al.*[41] applied a many-body potential approach to modeling a wide range of thermomechanical properties of actinide oxides, showing noticeable agreement with experimental results.

The study of the primary damage state (for example, point defects caused be a α-decay in UO_2) is essential to understand how the material ages. Molecular Dynamics (MD) simulations have also been successfully applied to model this phenomenon in various materials used in nuclear science applications.[42] Simulation techniques based on empirical potentials have been used in this sense,[43] focusing at first on pure uranium dioxide to describe the behavior of point defects but also estimate the elastic and melting properties. It could be, for example, determined that simple defects such as interstitials occupy the large, empty zone 4b in the unit cell. However, for positive deviation from stoichiometry, Willis determined that oxygen interstitials tend to form clusters, which have a binding energy of about 1.7 ± 0.6 eV.[44] The structure that best fitted experimental neutron diffraction patterns is a 2:2:2 cluster, consisting of two interstitials and two oxygen atoms displaced from their regular lattice position, creating two additional interstitials and two vacancies. This is illustrated in **Fig. 13**.[43]

The study on the formation of point defects via ab initio and Molecular Dynamics (MD) consider now also the behavior of oxygen, which is the fastest diffusing specie in UO_2 but nevertheless has an impact on many of the macroscopic properties, as it notably affects the transport properties.

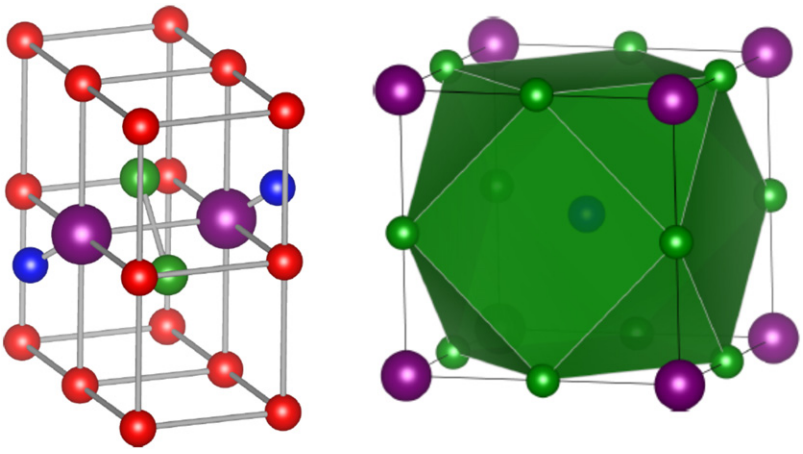

Fig. 13 Structure of the Willis cluster (left). Both oxygen interstitials (in green) occupy 48i sites corresponding to a displacement from the 4b site of ~ 1.1 Å along a <1 1 0> direction (purple lines). In addition, two oxygen atoms (in blue) are displaced by ~ 1.33 Å from their regular lattice (in purple) positions, along a <1 1 1> direction to 32 f sites. In a cuboctahedral configuration, 8 out of 12 oxygen atoms (green) are from the initial structure the 4 others and the one in the center (blue) are new (total of 5 oxygen atoms) without lattice volume change.

Table 2 Point defects energies in UO_2

Point defect	*Formation energy (eV)*			
	Bertolus[46]	Cooper[47]	Li[48]	Matzke[49]
Oxygen interstitial I_O	−0.05	–	−2.4	–
Uranium interstitial I_U	5.36	–	10.3	–
Oxygen vacancy V_O	5.38	–	6.3	–
Uranium vacancy V_U	10.43	–	7	–
Bound di-interstitial I_{OO}^{O}	0.43	–	–	–
Bound di-interstitial I_{OO}^{X}	−0.26	–	–	–
Bound Schottky defect S_1	3.32	–	–	–
Bound Schottky defect S_2	2.54	–	–	–
Bound Schottky defect S_3	2.82	–	–	
Infinitely separated Schottky defect S^*	10.66	11.6	8.1	6–7
Infinitely separated Oxygen Frenkel pair FP_O^*	5.33	5.7	5.3	3–4
Bound uranium Frenkel pair FP_U	11.18			
Infinitely separated uranium Frenkel pair FP_U^*	15.79	15.5	17.3	9.5

By using MD simulations, Devanathan[45] found that only about 1% of the displacements occur on the uranium sublattice, whereas oxygen Frenkel pairs are an order of magnitude more numerous than uranium Frenkel pairs in the primary damage state.

A comprehensive study of the transport properties of defects and fission gases in uranium dioxide can be found in the work of Bertolus *et al.*[46] and Cooper *et al.*[47] An empirical molecular dynamics potential in the Charge-Optimized Many-Body (COMB) formalism that covers the whole uranium-oxygen composition range has been developed recently and the formation energies determined[48] are also included in **Table 2** together with the experimental values determined by Matzke for the Frenkel pairs and Schottky defects.[49] **Table 2** below summarizes defects energies for UO_2 taken from the former sources.

2.05.3.4 Extended Defects

Once point defects start diffusing within the solid, they can interact with each other and form extended defects (linear, planar or three-dimensional defects) so as to reduce the total energy.

The following extended defects must be considered:

(1) Dislocation-type defects: In general, dislocation-type defects are loops which can exhibit edge, screw and mixed dislocation character within a single loop, or can be prismatic (interstitial- or vacancy-type dislocation loops). The latter is a direct consequence of production and diffusion of interstitials and vacancies of the U and O sublattices. The former is a plastic deformation under external loading and is not a direct product of the fission process.
(2) Voids: These are formed by vacancies absorption and are more stable than vacancy loops.
(3) Stacking faults: They form as a consequence of the movement of dislocations through the crystal, and result in a lattice plane displaced by a non-Bravais lattice vector. It was recently found[50] that ⟨110⟩ dislocation loops present no stacking fault, whereas ⟨111⟩ dislocation loops do.
(4) Grain boundaries: They consist of the junction of two crystallites differently oriented along a common planar surface, resulting in a polycrystalline material.

2.05.3.4.1 Dislocation loops

The geometry of slip in a single crystal is fully defined by the slip system, which designates the slip plane (reticular plane in which surface atomic density is maximum) and the slip direction (reticular direction in which linear atomic density is maximum). The dislocation is generally ca mixture of screw and edge components in the shape of a loop. However, important deformation properties, such as the creep rate and the yield stress (or usually called the critical resolved shear stress), are controlled primarily by the edge components of the dislocation. Consequently, the nature of edge dislocations in UO_2 has received most of the attention in the literature. In 1960, Rapperport and Huntress[51] examined the macroscopic slip of UO_2 single-crystals deformed by compression between 700°C and 1900°C. The most active slip system, highlighted by the analysis of slip trace and the Laue stereotypes, is $\{100\}<110>$. The $\{110\}$ and $\{111\}$ planes become active when the temperature increases, the slip direction remaining $<110>$. The planes $\{111\}$ are often activated by cross-slip. In 1963, Ashbee confirmed these results, by means of TEM observations, and defined the corresponding Burgers vector as $a/2<110>$.[52]

The distance $a/2<110>$ effectively corresponds to the shortest period of the fluorite network. Primary slip planes in UO_2 are not the densest ones, that is $\{111\}$ planes as classically observed in fcc metals. The most important slip system in UO_2 is the one which minimize the electrostatic energy rather than the elastic energy of the crystal. The easy slip along $\{100\}<110>$ tends to minimize the intense repulsive force between cations. The anions then act as a screen during such translations. The ionic

configurations of dislocations in UO_2 have been investigated by Evans[53] in order to identify the peculiarities that may influence the deformation characteristics of this material.

Ashbee[52] has observed dissociated dislocations in partial dislocations. However, these stacking faults might have been identified in non-stoichiometric UO_2 due to the TEM observation conditions which induced a local reduction of the oxide. These excess uranium ions could stabilize stacking faults according to calculations based on an ionic model.[54] The same calculations showed that the stacking fault energy was much too high to consider the dissociation of dislocations into partial dislocations in UO_2.

2.05.3.4.2 Prismatic loops

Another type of loop is called a prismatic loop. This type is fundamentally different from the shear loop; the only features they have in common is their circular shape and their ability to expand or contract radially. Fig. 14 shows a TEM micrograph of a UO_2 sample having cumulated 10^{-5} dpa α-damage. Prismatic dislocation loops are clearly visible in this sample. Studies have shown that the loops grow in size and concentration as a function of the α-damage.[28,55] Corresponding to the two types of point defects, vacancies and interstitials, there are two types of prismatic loops. The interstitial loop consists of a disc-shaped layer of atoms formed by assembling free interstitial atoms from the bulk solid. The atom-layer agglomeration is thermodynamically more stable than the same number of atoms dispersed in the lattice as self-interstitials. Interstitial loops generally form in solids bombarded by high energy radiation (e.g., fission fragments) because only this environment produce sufficient quantities of self-interstitials.

Recently, Onofri *et al.*[56] found for Xe implanted UO_2, dislocation loops 10–80 nm in size, faultless, prismatic, of interstitial type and with Burgers vectors only pertaining to $<110>$-type directions.

As in the case of the interstitial loop, the outer region of the vacancy loop is a circular edge dislocation with a Burgers vector perpendicular to the plane of the loop. However, the Burgers vectors of the two types of loop are of opposite sign. By definition, an interstitial loop grows/shrinks by absorption of interstitials/vacancies, whereas a vacancy loop grows/shrinks by absorption of vacancies/interstitials. However, vacancy loops shrink by self-interstitial atom absorption at all temperatures and by vacancy emission at high temperatures. This means that vacancy loops are intrinsically unstable at all temperatures. Rather than forming loops in the shape of a disc, vacancy condensation results in voids, which become in turn a perfect trap for gas atoms (see next paragraph and Fig. 15).

2.05.3.4.3 Void nucleation and growth

Because of preferential absorption of self-interstitials at dislocations, a slight excess of vacancies is left in the solid to first nucleate and then grow voids (a void does not contain gas initially). Voids, as well as prismatic loops, can nucleate either homogeneously or heterogeneously.

Homogeneous nucleation refers to the build-up of small clusters by casual interactions of individual point defects randomly moving through the solid. The stability of these clusters relative to the individual point defects of which they are composed (that is, voids contain vacancies and perhaps gas atoms, whereas loops contain interstitials) is the driving force for nucleation. In this case, no structural features (pre-existing gas bubbles, incoherent precipitate particles, dislocations) within the material are needed to cause agglomeration of the point defects. Heterogeneous nucleation refers to the formation of voids on the aforementioned structural features of the material. The depleted zone created in the collision cascade can also act as heterogeneous nucleation site for void formation. The latter is considered to be the most important nucleation mechanism in irradiated UO_2 fuels.[57]

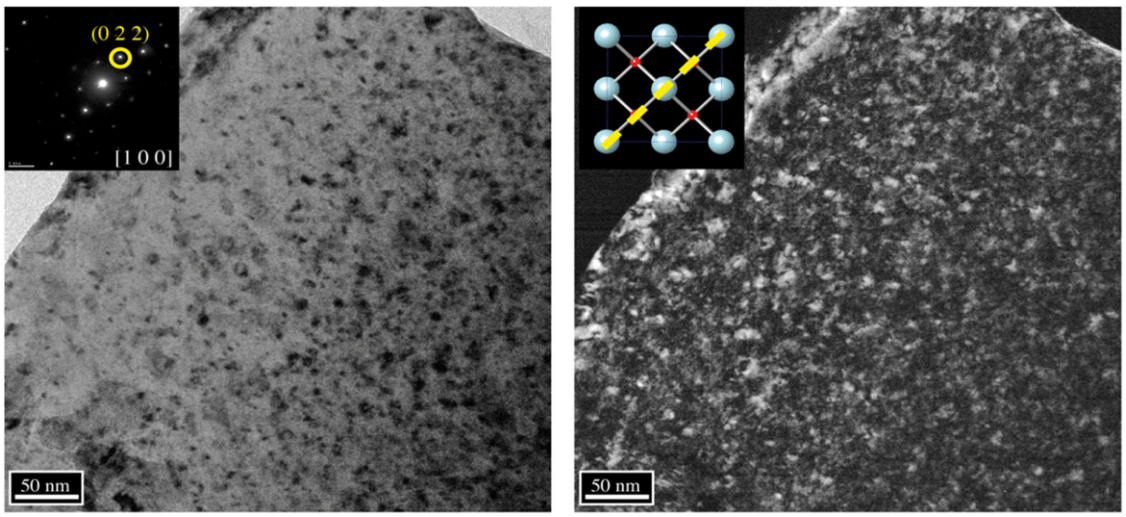

Fig. 14 TEM micrographs of 10 wt% ^{238}Pu-doped UO_2 showing the presence of prismatic loops resulting from the α-damage. The left micrograph shows a bright field image and the selected spot from the diffraction to produce the dark field image on the right. With permission of the European communities. © European Atomic Energy Community.

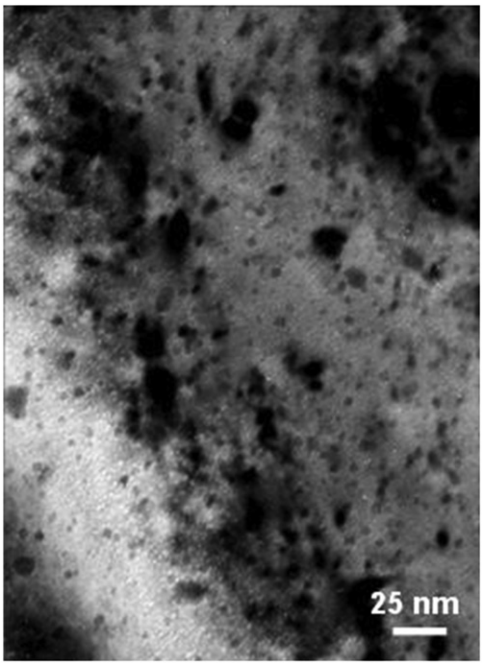

Fig. 15 TEM micrograph of a 10 wt% ^{238}Pu-doped UO_2 (0.4 dpa) showing void (bright spots) formation from the α-damage. With permission of the European communities. © European Atomic Energy Community.

Nucleation and growth are often treated as sequential steps in the overall process of void formation. During the nucleation period, the density of cavities increases with time, but their size remains small. During the growth period that follows, their density stabilizes whereas their size increases with time. The void is assumed to be spherical and its growth is controlled by diffusion of vacancies and interstitials from the bulk of the solid to the void surface. In most situations, gas atoms will stabilize the voids/cavities. **Fig. 15** shows a TEM image from an α-damaged (U, Pu)O_2 sample where voids have formed by diffusion of vacancies and are eventually stabilized by the radiogenic helium. The corresponding interstitial loops formed, visible in **Fig. 14**, have been annealed. Similar effects have been recently observed (and modeled by classical molecular dynamics) in ion implanted UO_2 samples, despite the fact that no gas is infused and no cation diffusion is expected.[58–60]

2.05.4 Radiation Effects in UO_2 and in UO_2 Based Fuels

Most electricity-producing nuclear power stations use uranium dioxide (UO_2) enriched in ^{235}U to about 5% as fuel, whereas some also use MOX (mixed oxide) fuel, that is, UO_2 with about 8.5% of PuO_2.[61] The fuel consists of sintered pellets of about 1 cm in diameter. These pellets are used to produce long stacks that are sheathed in tubes (cladding) of a Zr alloy.

Uranium dioxide fuel is exposed to all the radiation and damaging sources, including γ and X-rays, neutrons, electrons, fission fragments, and α-decaying elements, for about 5 years. During this period, the amount of FPs grow inside the fuel and change both chemical and physical properties. Any treatment of damage effects has to allow for such changes that occur even in the absence of damage build-up. Also, fuel activity does not stop after irradiation, in the short term due to the β- and γ-decay of FPs but, in the long term, mostly because of the continuous α–disintegration of the actinides.

2.05.4.1 Change in Chemical Properties

When discussing damage accumulated by fission or, to a lesser extent, by radioactive decay, one has to consider the simultaneous change in chemistry. Each fission, besides producing the above mentioned 100,000 displacements, also yields two FPs, often amounting up to more than 3 at% at the end of life of the commercial nuclear fuels. The FPs include gaseous elements like Kr, Xe, volatile elements such as Br, I, Cs, metals such as Mo, Ru, Pd, Rh, and Tc (which may form precipitates known as ε-particles) and Ba and Zr, which may form ceramic compounds.[62]

Since most of the FPs decay by β- and γ-emission with rather short half-lives, new elements are formed, particularly during the active life of the fuel but also, to a lesser extent, once the fuel is in storage (with the exception of very few, long-lived FPs: e.g., ^{129}I).

For example, Cs, a highly abundant fission product, decays to Ba with another valence state and a different chemical behavior. Gaseous helium is also formed by the α-decay of short-lived resulting actinides, e.g., ^{241}Am which decays to ^{237}Np. We are therefore dealing with complex phenomena, which explains why it is very important to account for compositional changes when

studying damage effects and mechanisms, not only in conventional nuclear fuels (despite the large amount of work devoted to this subject in the past five decades) but also in innovative fuels. For instance, an extensive review of chemical changes in irradiated fast reactor fuels (with higher burn-up and higher operating temperatures) can be found in Parrish *et al.*[63]

2.05.4.2 Change in Bulk Physical Properties

The physical effects caused by atomic displacements are rather complex and depend on the relative sink strengths of a given material for interstitials and vacancies and on the temperature. A majority of the Frenkel pairs recombine in a short time. The defects that survive migrate through the crystal lattice where they cluster to form extended defects like dislocation loops, lines and networks, which can potentially be absorbed in grain boundaries, gas bubbles or precipitates, which act as sinks.

One of the major effects of defect formation is the degradation of thermal diffusivity, due to phonon scattering. Results obtained on irradiated UO_2 show that the thermal conductivity is decreasing with increasing burn-up, and that at equal burn-up, samples with higher irradiation temperatures have higher thermal conductivity.[64,65] This result highlights the correlation between magnitude of damage generated by increasing burn-ups and thermal conductivity. It also shows that annealing at high temperatures reduces the amount of defects, in turn diminishing the thermal diffusivity degradation.

Another important effect of radiation damage is the volume increase of the crystal lattice, leading to macroscopic swelling of the fuel material. Dopants, in the form of short α-decaying isotopes, have been added to UO_2 to generate substantial amount of damage in a laboratory compatible period of time. For example, at room temperature α-damage in UO_2 doped with ^{238}Pu leads to a clear increase of the volume, which quickly reaches saturation, until equilibrium between formation and annealing of defects is attained (see **Fig. 16** below).

In this case, the ingrowth or the change in the lattice parameter of UO_2 doped with ^{238}Pu, leading to an increase in volume, is reflecting the evolution of radiation damage. Accumulation of radiation damage can also lead to phase changes. It can result in either amorphization (also called metamictization[66] of originally crystalline matter, or polygonization). The latter describe the rearrangement of those dislocations formed in the earlier stage of irradiation that do not annihilate one another, into walls of dislocations, forming low-energy "sub-boundaries" and perfect but slightly misaligned sub-grains. It occurs in some nuclear fuels at high burn-up (expressed in GWd/tU or in percent fissions of the heavy metal atoms); in the case of UO_2 fuel, about 10^{-4} sub-grains are formed from each original grain. This phenomenon was already observed in early test irradiations and was called grain subdivision.[67] It received renewed attention in the 1980s, when power reactors increased the fuel burn-up.[68] Polygonization has also been observed in ion implanted UO_2.[69] No experimental evidence of amorphisation was ever observed, even for high fluence implanted UO_2, in agreement with MD calculations.[70]

The understanding of the basic processes involved in the damage build-up could also help to predict the long-term behavior of UO_2 (nuclear fuel) during storage (either interim or in the long term). Between 130 and 1000 °C, the diffusion of U and Pu atoms is completely athermal, that is, independent of temperature. The results have been explained by the formation of thermal spikes along the trajectory of the fission fragments in combination with a pressure gradient. Because of the high-energy deposition rate, a locally (over)heated track (fission spike or thermal spike) may form. Such fission tracks have been observed in transmission electron microscopy in irradiated UO_2 with the replica technique at UO_2 surfaces, but not in TEM samples prepared from the bulk.[16,17] High energetic ion tracks, however, have been observed in ion irradiated UO_2. It was found that the threshold for the formation of observable tracks must be near to the energy loss value of FPs, that is 18–22 keV/nm.[33,71]

An extreme case of fission spikes interacting with the fuel matrix is the destruction of pre-existing fission gas bubbles by a fission spike that is passing by. The phenomenon is called "re-solution" of fission gas and was known for about 40 years

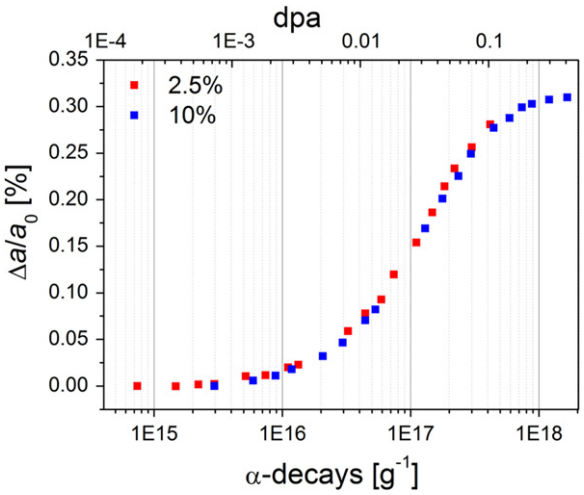

Fig. 16 Lattice parameter evolution as function of accumulated α-damage (dose) for two UO_2 samples doped with 2.5 and 10 wt% of ^{238}Pu, respectively. With permission of the European communities. © European Atomic Energy Community.

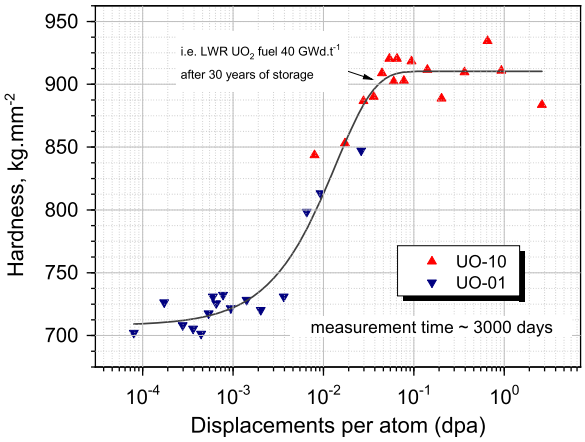

Fig. 17 Hardness evolution for two α-doped materials expressed as a function of accumulated damage (dpa). With permission of the European communities. © European Atomic Energy Community.

(see Fig. 5). It was explained by the above-mentioned hydrostatic pressure component[19] of the thermoelastic stress field of the fission spike interacting with the bubbles. The pressure gradients also explain the surprisingly high U and Pu diffusion coefficients. To decrease these gradients, the highly mobile uranium interstitials are pushed away from the spike axis, thus increasing the U-diffusion to values higher than those calculated accounting only for atomic mixing and thermal spike effects.

Like diffusion, in-pile creep in UO_2 was shown to be athermal and fission-enhanced below 1273K as well.[72] However, for higher temperatures two different regimes are observed: at high stress levels creep rate follows a power law, due to a dislocation diffusion mechanism, whereas for lower stresses cation diffusion controls it, following a linear diffusion flow law.[73]

Mechanical properties can also vary as a function of damage cumulating in UO_2. Fig. 17 shows the evolution of the Vickers hardness as function of accumulated damage for two differently α-doped compounds.

The accumulated decay damage differs by two orders of magnitude, whereas the combined data for the two materials span over six orders of magnitudes, providing an insight on the different stages of radiation damage accumulation. The initial trend for the UO_2 doped with 0.1 wt% of ^{238}Pu shows essentially no clear changes of the hardness. A relatively sharp transition occurs around 10^{-2} dpa, indicating that this is a threshold level at which the accumulation of microscopic defects produces evident macroscopic changes. This level of damage corresponds to spent fuel at discharge time from the reactor or during the first months/years of cooling. This is true if one assumes that the irradiation in reactor, at higher temperature (especially in the central part), had as an effect comparable to a thermal treatment, resulting in the annealing of most of the defects of the same type than those produced by α-decay.

In spite of the different decay rates, the evolution of the hardness shows an essentially continuous evolution, independent from the time necessary to reach a given displacements per atom (dpa) level. This important result is confirmed by other types of analyzes.

TEM microstructure analyzes revealed that damage accumulation up to a few dpa is characterized by the production of dislocation loops, as shown in Fig. 14. More recently, the evolution of the lattice parameter was shown to be independent from the concentration of the α-emitters but directly related to the damage level as shown in Fig. 16.

2.05.4.3 Elastic Properties

Among the physical properties affected by radiation damage, elasticity is of paramount importance, since it has a direct effect on the thermo-mechanical behavior of the fuel. It has been found recently that Young's modulus decreases with increased damage, both for auto irradiated and heavy ion implanted specimens; in the former case, however, an increase was detected starting at very high ($>$ 5 dpa) damage levels, which was explained with an increase in the number of extended defects leading to partial relaxation of the material.[74] In the case of irradiated fuels, it could be shown that the elastic modulus decreases with increasing burnup, as shown in Fig. 18.

Similar results were obtained by Terrani *et al.*,[75] who reported a decrease of the Young's modulus as a function of local burnup in the range of 60–130 MWd/kgU.

2.05.4.4 The High Burnup Structure

In the late 1950s, it was observed that a strong capture of neutrons by ^{238}U in the resonance range occurs at the periphery of the nuclear fuel, leading to the production of ^{239}Np and therefore of ^{239}Pu.[76] The consequence of the increase of the fissile density is a local increase of the burnup. The area concerned by this phenomenon is typically the annular outer part of the fuel pellet, about 200 μm in thickness, representing about 8% of the fuel (with average 60 MWd kgU^{-1} burnup). The local enrichment then decreases almost exponentially toward the center of the fuel. The original grains, with an average size of around 10 μm in typical Light Water Reactors (LWR) fuels, tend to subdivide into thousands of smaller grains about 100–200 nm in size. This restructuring

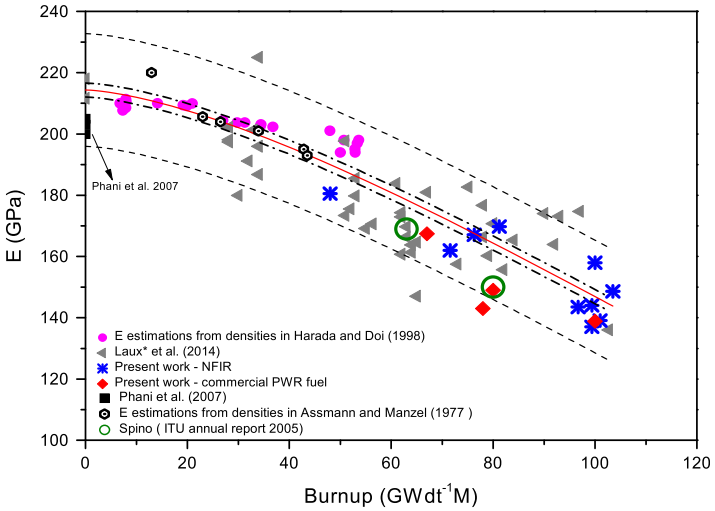

Fig. 18 Young modulus as a function of burnup. From Marchetti, M., *et al.*, 2017. Physical and mechanical characterization of irradiated uranium dioxide with a broad burnup range and different dopants using acoustic microscopy. J. Nucl. Mater. 494, 322–329.

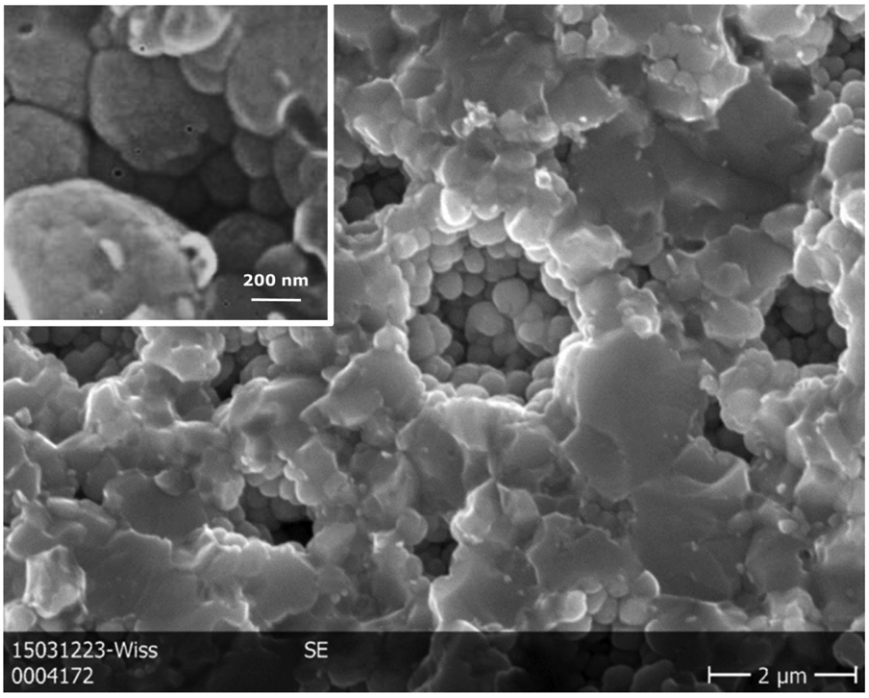

Fig. 19 Secondary electron image of a restructured UO_2 fuel (200 GW_d t^{-1} local burnup) showing the occurrence of rounded shaped sub-grains inside pores. The insert is a higher magnification detail of a pore showing the fractal nature of the subgrains. With permission of the European communities. © European Atomic Energy Community.

of the grains is associated with the formation of a local porosity that can reach values above 20%. The coarsened, micrometric sized pores contain almost all of the fission gases. For power reactors, this phenomenon has been observed in the 1980s. Two different structures, rounded grains at open surfaces and (bulk) polyhedral grains, have been identified in the high-burnup region of the fuel.[77] The formation of smaller grains at open surfaces (e.g., pores) shows a fractal appearance with the smaller grains having a size of less than 10 nm, as can be seen in the Scanning Electron Microscopy (SEM) image of **Fig. 19**, particularly in the higher magnification image in the inset.[78]

The surface reorganization has been observed by SEM[79,80] and is accompanied by a bulk restructuring which, although observable by SEM, is mostly investigated by TEM analysis.[81] The fuel transforms by a sub-division process in polyhedral grains surrounding pores. The newly formed tiny grains are often found to be slightly misoriented by a few degrees.[82] Hiernaut *et al.* reported observing a pattern

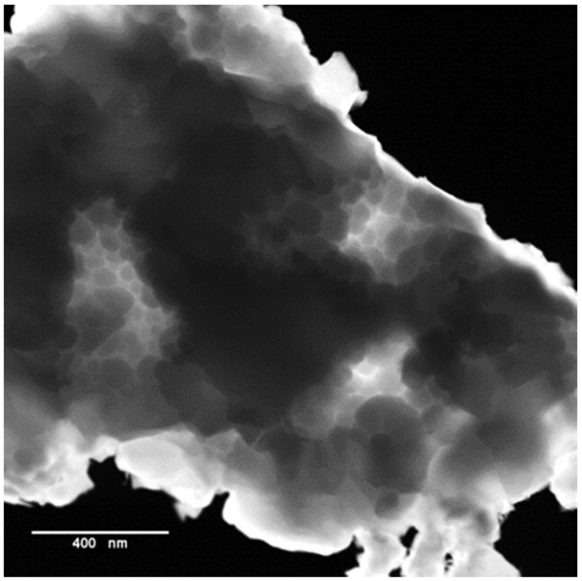

Fig. 20 TEM micrograph of a fuel sample irradiated at 100 $GW_d\ t_U^{-1}$. With permission of the European communities. © European Atomic Energy Community.

which suggests a "memory effect" with respect to the initial grain structure of the un-irradiated material, which in turn seems to support this assumption.[83] **Fig. 20** shows a TEM image of a high burnup UO_2 fuel sample (100 GWd/t_U^{-1}) showing the formation of the High Burnup Structure (HBS). The bright field image allows distinguishing rounded and polyhedral grains.

The exact mechanisms responsible for the formation of the HBS are still under investigation. The formation of defects in combination with the presence of fission gases appears to play a key role in the process and several scenarios have been suggested.[84]

Nogita and Une[85,86] proposed a formation mechanism of the HBS that is directly related to the accumulation of radiation damage. Tangled dislocation networks are formed by the inhomogeneous accumulation of dislocations after the development of interstitial-type dislocation loops. At the same time, intragranular FPs gas bubbles are formed by the clustering of either vacancies or fission gases (Xe and Kr). With increasing burn-up, tangled dislocations are organized into sub-divided grains with high angle boundaries.[85] Then, some of them are recrystallized, sweeping out small intragranular bubbles. In this approach, recrystallization, and therefore HBS formation, consists of a series of steps, that is formation of sub-grains, growth of the sub-grains into recrystallization nuclei, and growth of the recrystallized grains. In line with this hypothesis, Spino *et al.*[87] have tentatively attributed the formation of the HBS to the local beginning of recrystallization around pores (characteristic of the HBS). This interpretation has been confuted by the results of the High Burnup Rim Project (HBRP), in which a set of irradiated UO_2 disks of different burnup and temperature conditions were analyzed extensively.[88]

TEM observations of HBRP samples[89] showed that in the HBS the initial grains are sub-divided and not recrystallized. **Figs. 19** and **20** show SEM and TEM images of re-structured UO_2 fuel samples. The sub-divided grains, some as small as 50 nm, are clearly visible. The subdivision process proceeds further with increasing burnup as observed by the SEM examination of a very high burnup specimen.[83] Sonoda *et al.*[89] thus concluded that the restructuring is initiated by the accumulation and mutual interaction of several effects: (1) radiation damage including point defects and dislocations, (2) formation of FPs including gas bubbles and metal particles, (3) stored energy caused by electronic excitation and nuclear collisions which may cause radiation-enhanced diffusion of interstitials and vacancies, and (4) growth of dislocation loops.

Lozano *et al.*[77] observed both round and polyhedral subgrains in HBS. The former, with an average size around 0.1 μm, were found around coarsened pores or at free surfaces whereas the latter, ranging up to 0.8 μm, appeared mostly in the bulk region.

In a more recent study, Gerczak *et al.*[90] investigated a near complete cross-section of high burnup commercial UO_2 fuel from the fuel-cladding interface to near the fuel pellet center, observing distinct microstructural regions (see **Fig. 21**). They concluded that the onset of restructuring resulting in HBS formation at the pellet rim is marked with the formation of Low Angle Grain Boundaries (LAGBs), which in turn is indicative of polygonization.

This process ultimately results in a completely restructured zone with a majority of high angle GBs.

The polygonization process was also recently evidenced in 84 MeV Xe-irradiated UO_2 samples.[91] Several authors reported evidence of the formation of micrograins, both close to the rim and at intermediate places within the pellet of high burn-up fuel. Manzel and Walker[92] maintain that the latter are an extension of the HBS from the pellet rim, whereas the results from Noirot *et al.*[93,94] suggest a new, submicron sized grain population with orientations dispersed around that of the original grains and separated from the rim HBS (the same effect visible in **Fig. 20** in the case of $r/r_0 = 0.35$). In these restructured pellet centers, the intragranular fission gas bubbles detected at low magnification by SEM and optical microscopy are mostly on the boundaries between these submicron sized grains, and their shapes are far from spherical and often more complex than simple lenticular bubbles.

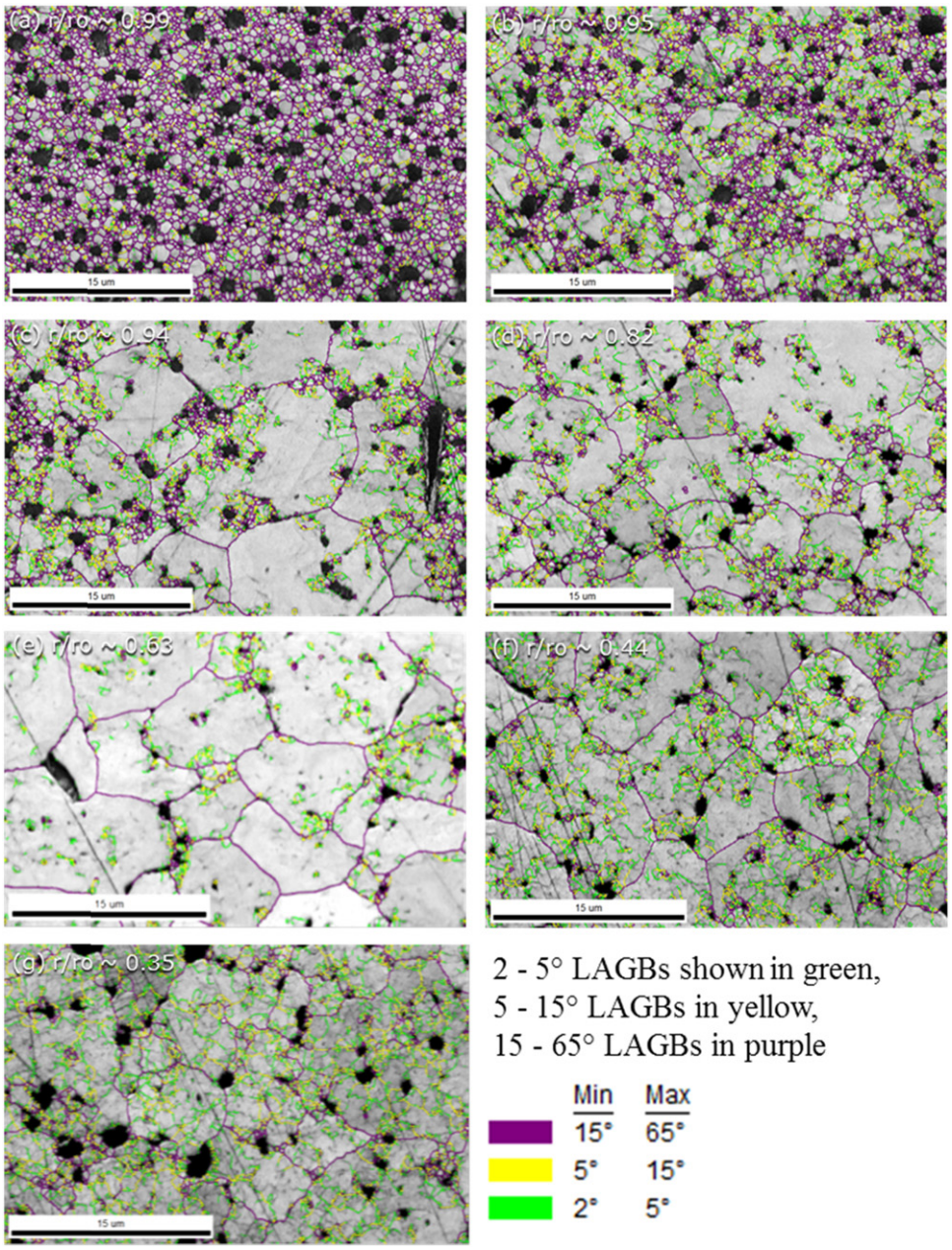

Fig. 21 EBSD grain boundary misorientation map moving from the fuel-cladding interface (top left corner) to close to the fuel center (bottom right). From Gerczak, T.J., *et al.*, 2018. Restructuring in high burnup UO_2 studied using modern electron microscopy. J. Nucl. Mater. 509, 245–259.

Despite the different views on its formation mechanism, there is now agreement that the HBS has a high fission gas retention capacity. In particular, the HBS does not evolve toward an open system of interconnected channels, even when porosity reaches very high values (e.g., 35% in an FBR fuel, 50% in a PWR MOX agglomerate).[95]

A major question, however, remains: how can these middle sized micro-grains allow release of gas atoms from the fuel whereas micro-grains in the HBS at the pellet rim allow the formation of micron size pores but no release.[96] Advanced analysis tools such as high resolution TEM, in conjunction with FIB and EBSD, could be the key to finding an answer in the near future.

Jegou *et al.*[97] investigated irradiated UO_2 by Raman spectroscopy, evidencing Raman lines characteristic of irradiation-induced defects. Their results seem to confirm that high burnup structures have a better oxidation resistance. In plutonium enriched agglomerates found in MIMAS MOX irradiated fuels, the stabilizing effect (preserving the fluorite structure) can be explained by the high plutonium content of these agglomerates, although the increase in fission product concentration also contributes. The better oxidation resistance of the rim zone, as compared to the grains in the central zone, of a UO_2 fuel with 60 $GW_d\ tU^{-1}$ supplies more evidence on the beneficial effect of FPs in terms of retarding oxidation.

In any case, as a technological consequence of this result, the HBS would appear to effectively retain the fission gases occluded in pores up to relatively high local burn-ups (>300 MWd/kgHM) since only at these burnup values porosity fractions greater than 0.3 may be reached.

As mentioned in Section 2.05.3.2, the formation of HBS considerably affects the thermal conductivity; in particular, it was found that this physical parameter decreases with increasing burn-up, due to the accumulation of defects in the crystalline lattice.[98] A thorough, in-pile study by Ronchi *et al.*[99] concluded that HBS actually causes a slight increase in the intrinsic conductivity, due to the lower amount of defects in the newly formed structure. Therefore, high burn-up fuels will run cooler in the reactor than one would expect from its thermal conductivity versus porosity behavior at low burnup, therefore leading to lower fission gas release.

In the next article, we will discuss a possible mechanism for this behavior.

2.05.4.5 Can Polarons Explain the Radiation Resistance of UO_2?

It is well known that UO_2 is far more resistant to radiation damage when compared to other ceramic oxides of similar structure.

An early analysis of the conduction mechanism in nearly stoichiometric UO_2 single crystals was performed by de Coninck,[100] who suggested the electric carriers to be polarons, defined as charge carriers coupled to phonons (see **Fig. 22**, taken from,[101] for a graphic representation of the defect).

Since then, several studies have confirmed that polarons increase the heat capacity, the thermal expansion coefficient and the electric conductivity of UO_2.[102]

This in turn results in an unusually high threshold value for amorphisation, as defined by Szenes.[103] In his paper, he describes the formation of tracks resulting from a thermal spike. Two main approaches describing thermal spike effects in UO_2 were proposed by Szenes[104] and Toulemonde[14] differing mainly by the initial state of propagation of the heat from the high energetic ions. The thermal properties of the material at the extreme temperature of the spike remain important to assess the level of damage (track size) in the two temperatures model of Toulemonde.

Baldinozzi *et al.*[105] determined that an increase of the specific heat of the sample has, generally, a favorable impact on the radiation resistance of the system because it can react to irradiation storing the energy of the impinging ion in a more efficient way before melting. Polarons, unlike electrons that have no significant contribution to the specific heat of a crystal at high temperature, provide extra degrees of freedom to the system that are readily available.

The heat capacity of UO_2 unexpectedly increases from around 1000K, which can be fitted by empirical laws but is still not fully understood. Possible explanation relate this behavior to the formation of defects, either polarons[106] or oxygen Frenkel pairs.[107]

Desgranges *et al.*[108] predicted that, within the framework of the thermal spike model above mentioned, the high temperature properties of UO_2 are strongly affected by the presence of thermally activated polarons, which increase the heat capacity, the thermal expansion coefficient and the electric conductivity.

The thermal diffusivity and heat capacity of uranium dioxide was measured between 500 and 2900K by Ronchi *et al.*,[99] who found that the heat capacity continues to increase even at temperatures above the expected lambda transition (~2670K).

More recently, a new set of measurements of heat capacity, thermal conductivity and thermal diffusivity of UO_2 have been presented in the temperature range 1500–2900K.[102] The authors observed a similar transition in heat capacity, which was explained in terms of a competition between oxygen defect interactions (attraction of oppositely charged defects) and saturation of oxygen interstitial sites.

They also concluded that at temperatures above 2000K, although oxygen defects contribute to electrical conductivity, polaron mobility remains the dominant mechanism for electrical charge transport due to their significantly lower activation energy compared to oxygen vacancies and interstitials.

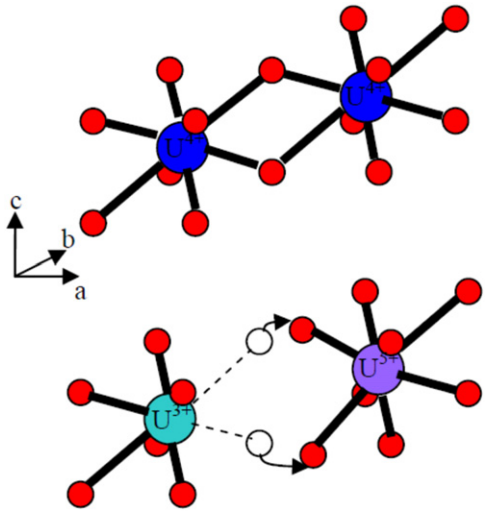

Fig. 22 Schematic drawing of a UO_2 regular lattice (top) and a polaron containing lattice (bottom).

In conclusion, polarons seem to greatly influence the high temperature thermal behavior of UO_2, although a clear understanding of the mechanism is still lacking.

2.05.5 Conclusions and Perspectives

Radiation damage in UO_2 has been extensively studied for more than 50 years. The studies cover single effects from various damage sources up to combined effects in, e.g., irradiated nuclear fuels. UO_2 is the most commonly used fuel in nuclear reactors and a thorough knowledge of its behavior under irradiation is extremely important to ensure a safe exploitation of this energy production source. Safety and economic issues have given a strong impulse to research on the microstructural evolution of the fuel at high burnup.

Modern analytical techniques (RAMAN, HR-TEM, APT, EXAFS, EELS, etc.) applied to UO_2 in combination with atomistic modeling and meso-scale modeling should also allow filling the gap in the comprehension of the damage formation and effects in this material.

The second practical issue related to understanding damage formation in UO_2 lies in predicting its long-term behavior especially when used as nuclear fuel. The spent fuel to be disposed of will not be in equilibrium, due to radioactive decay lasting thousands of years. The α-damage will impact the long term properties of the spent fuel, so that it is of paramount importance to comprehend the mechanisms of damage formation in order to predict its behavior. In particular, the combination of radiogenic helium formation and substantial α-damage might superpose to the already damaged irradiated fuel. The hotter part of the fuel during irradiation might have experienced annealing of most defects so that α-damage occurring at storage temperature might result in swelling of these parts of the fuel. Irradiation temperature gradient would definitely results in different damaged state along the radius of a fuel pellet so that isotropic swelling could cause stresses in the fuel.

Recycling reactor-grade plutonium back into the same or a more advanced fleet of reactors was widely regarded as the best choice in the 1960s, since at the time the uranium market was anticipated to become crowded and supplies tight. Nowadays, however, due to the discovery of new uranium ores the issue has become less stringent (in economic terms, relying only on fresh fuel nowadays remains cheaper than recycling).

Nevertheless, the need remains to consistently reduced Pu stockpiles, for both environmental and proliferation issues. Youinou and Vasile proposed the use of Pu together with enriched U, so that the Pu degradation of LWR fuels is compensated by an increase of ^{235}U enrichment.[109]

In the specific case of fast reactors, another important aspect of understanding the long-term evolution of nuclear fuels is linked to the present trend for MOX fuel development, which aims at making the fuel highly versatile in order to consume large amounts of Pu and transuranic species otherwise deposited in long term storage. Therefore, fuels must be able to operate up to high burnup states with Pu loading in the range of 30–40 wt%.

A comprehensive understanding of fuels (UO_2, MOX, Minor Actinide Bearing Blankets) microstructures and properties is therefore necessary for safe and efficient operation, requiring a thorough understanding of fuel behavior directly related to radiation effects at each point in the fuel life cycle.

See also: 1.02 Fundamental Point Defect Properties in Ceramics. 1.16 Ab Initio Electronic Structure Calculations for Nuclear Materials. 1.20 Primary Radiation Damage Formation in Solids

References

1. Belle, J., 1961. Uranium Dioxide: Properties and Nuclear Applications. Washington: Naval Reactors, Division of Reactor Development, U.S. Atomic Energy Commission, (N.R. Handbooks).
2. Lemaignan, C., 2004. Science des Matériaux pour le Nucléaire. In Collection Génie Atomique. EDP Sciences.
3. Olander, D., 1976. Fundamental Aspects of Nuclear Fuel Elements. Springfield, VA: Office of Public Affairs Energy Research and Development Administration.
4. Curie, M.P., 1900. Comptes Rendus 130, 76.
5. Rutherford, E., Owens, R.B., 1899. Thorium and uranium radiation. Trans. R. Soc. Can. 2, 9–12.
6. Thomson, J.J., 1897. XL. Cathode Rays. Lond. Edinb. Dublin Philos. Mag. J. Sci. 44 (269), 293–316.
7. Rutherford, E., 1913. Radioactive Substances and Their Radiations. Cambridge: The University press.
8. Bohr, N., 1913. I. On the constitution of atoms and molecules. Lond. Edinb. Dublin Philos. Mag. J. Sci. 26 (151), 1–25.
9. Ziegler, J.F., Biersack, J.P., Littmark, U., 1985. The Stopping and Range of Ions in Solids. Oxford: Pergamon Press.
10. Soullard, J., Alamo, A., 1978. Radiat. Eff. 38, 133.
11. Martin, G., *et al.*, 2014. A thermal modelling of displacement cascades in uranium dioxide. Nucl. Instrum. Methods Phys. Res. Sect. B: Beam Interact. Mater. At. 327, 108–112.
12. Fleischer, R., Price, P., Walker, R. (Eds.), 1975. Nuclear Tracks in Solids. Berkeley: University of California Press.
13. Seitz, F., Koehler, J., 1956. Solid State Phys. 2, 305.
14. Toulemonde, M., Paumier, E., Dufour, C., 1993. Radiat. Eff. Solids 126, 205.
15. Baranov, I.A., *et al.*, 1988. Sov. Phys. Usp. 31, 1015.
16. Wiss, T., *et al.*, 1997. Swift heavy ion damage in UO_2. Nucl. Instrum. Method Phys. Res. B 122, 583.
17. Ronchi, C., 1973. J. Appl. Phys. 44, 455.
18. Matzke, H., 1983. Radiat. Eff. 75, 317.

19. Blank, H., Matzke, H., 1973. Radiat. Eff. 17, 57–64.
20. Ishikawa, N., *et al.*, 2013. Electronic stopping power dependence of ion-track size in UO_2 irradiated with heavy ions in the energy range of 1 MeV/u. Nucl. Instrum. Methods Phys. Res. Sect. B-Beam Interact. Mater. At. 314, 180–184.
21. Weber, W., 1984. Alpha-irradiation damage in CeO_2, UO_2 and PuO_2. Radiat. Eff. 83, 145–156.
22. Ronchi, C., Wiss, T., 2002. Fission-fragment spikes in uranium dioxide. J. Appl. Phys. 92 (10), 5837–5848.
23. Thomé, L., *et al.*, 2013. Combined effects of nuclear and electronic energy losses in solids irradiated with a dual-ion beam. Appl. Phys. Lett. 102 (14), 6.
24. Gutierrez, G., *et al.*, 2019. Effect of coupled electronic and nuclear energy deposition on strain and stress levels in UO_2. J. Nucl. Mater. 519, 52–56.
25. Matzke, H., Meyer, O., Turos, A., 1991. Damage recovery in the U-sublattice of ion implanted UO_2 between 5K and 2000K. Radiat. Eff. Defects Solids 119–121, 885–890.
26. Weber, W.J., 1981. Ingrowth of lattice defects in alpha irradiated UO_2 single crystals. J. Nucl. Mater. 98 (1–2), 206–215.
27. Weber, W.J., 1983. Thermal recovery of lattice defects in alpha-irradiated UO_2 crystals. J. Nucl. Mater. 114 (2–3), 213–221.
28. Staicu, D., *et al.*, 2010. Impact of auto-irradiation on the thermophysical properties of oxide nuclear reactor fuels. J. Nucl. Mater. 397, 8–18.
29. Rondinella, V.V., *et al.*, 1999. Mat. Res. Soc. Symp. Proc. 556, 447–454.
30. Rondinella, V.V., *et al.*, 2005. Studies on spent fuel alterations during storage and effects on corrosion behaviour. In: Proceedings of the 10th International Conference on Environmental Remediation and Radioactive Waste Management, ICEM'05. Glasgow.
31. Rondinella, V.V., *et al.*, 2007. Dose rate effects on the accumulation of radiation damage. In ICEM'07: The 11th International Conference on Radioactive Waste Management and Environmental Remediation. Oud Sint-Jan Hospital Conference Center. Bruges.
32. Wiss, T., *et al.*, 2014. Evolution of spent fuel in dry storage conditions for millennia and beyond. J. Nucl. Mater. 451, 198–206.
33. Matzke, H., Lucuta, P.G., Wiss, T., 2000. Swift heavy ion and fission damage effects in UO_2. Nucl. Instrum. Methods Phys. Res. Sect. B-Beam Interact. Mater. At. 166, 920–926.
34. Huang, M., Schwen, D., Averback, R.S., 2010. Molecular dynamic simulation of fission fragment induced thermal spikes in UO_2: Sputtering and bubble re-solution. J. Nucl. Mater. 399 (2), 175–180.
35. Vathonne, E., *et al.*, 2014. DFT + Uinvestigation of charged point defects and clusters in UO_2. J. Phys.: Condens. Matter 26 (32), 325501
36. Crocombette, J.-P., 2012. Influence of charge states on energies of point defects and clusters in uranium dioxide. Physical Review B 85 (14), 144101
37. Lidiard, A., 1966. J. Nucl. Mater. 19, 106.
38. Freyss, M., Petit, T., Crocombette, J.-P., 2005. Point defects in uranium dioxide: ab initio pseudopotential approach in the generalized gradient approximation. J. Nucl. Mater. 347 (1–2), 44–51.
39. Yakub, E., Ronchi, C., Staicu, D., 2009. Computer simulation of defects formation and equilibrium in non-stoichiometric uranium dioxide. J. Nucl. Mater. 389 (1), 119–126.
40. Soulié, A., *et al.*, 2018. Influence of vibrational entropy on the concentrations of oxygen interstitial clusters and uranium vacancies in nonstoichiometric UO_2. Phys. Rev. Mater. 2 (8), 083607
41. Cooper, M.W.D., Murphy, S.T., Andersson, D.A., 2018. The defect chemistry of $UO_{2\pm x}$ from atomistic simulations. J. Nucl. Mater. 504, 251–260.
42. Freyss, M., Vergnet, N., Petit, T., 2006. Ab initio modeling of the behavior of helium and xenon in actinide dioxide nuclear fuels. J. Nucl. Mater. 352 (1–3), 144–150.
43. Govers, K., 2008. Atomic scale simulations of noble gases behaviour in uranium dioxide. In Faculté des sciences appliquées. Bruxelles: Université Libre de Bruxelles.
44. Willis, B.T.M., 1987. J. Chem. Soc. Faraday Trans. 2, 1073.
45. Devanathan, R., 2017. Molecular dynamics simulation of fission fragment damage in nuclear fuel and surrogate material. MRS Adv. 2 (21–22), 1225–1230.
46. Bertolus, M., *et al.*, 2015. Linking atomic and mesoscopic scales for the modelling of the transport properties of uranium dioxide under irradiation. J. Nucl. Mater. 462, 475–495.
47. Cooper, M.W.D., Rushton, M.J.D., Grimes, R.W., 2014. A many-body potential approach to modelling the thermomechanical properties of actinide oxides. J. Phys.: Condens. Matter 26 (10), 105401
48. Li, Y., 2019. A universal COMB potential for the whole composition range of the uraniumoxygen system. J. Nucl. Mater. 513, 102–119.
49. Matzke, H., 1987. J. Chem. Soc. Faraday Trans. 2 83, 1121–1142.
50. Le Prioux, A., *et al.*, 2016. Empirical potential simulations of interstitial dislocation loops in uranium dioxide. J. Nucl. Mater. 479, 576–584.
51. Rapperport, E.J., Huntress, A.M., 1960. Deformation Modes of Singlecrystal Uranium Dioxide from 700°C to 1900°C. United States Atomic Energy Commission. pp. 1–29.
52. Ashbee, K.H.G., 1964. Stacking faults in uranium dioxide. Proc. R. Soc. Lond. 37–46.
53. Evans, A.G., Pratt, P.L., 1969. Dislocations in the fluorite structure. Philos. Mag. 20, 1213–1237.
54. Lefebvre, J.M., *et al.*, 1976. Calcul d'énergie de fautes d'empilement dans le dioxide d'uranium. J. Nucl. Mater. 60, 59–65.
55. Jonnet, J., *et al.*, 2008. Growth mechanisms of interstitial loops in α-doped UO_2 samples. Nucl. Instrum. Methods Phys. Res. Sect. B: Beam Interact. Mater. At. 266 (12–13), 3008–3012.
56. Onofri, C., *et al.*, 2017. Full characterization of dislocations in ion-irradiated polycrystalline UO_2. J. Nucl. Mater. 494, 252–259.
57. Martin, G., *et al.*, 2010. Irradiation-induced heterogeneous nucleation in uranium dioxide. Phys. Lett. A 374 (30), 3038–3041.
58. Maillard, S., Martin, G., Sabathier, C., 2016. Why a steady state void size distribution in irradiated UO_2? A modeling approach. Nucl. Instrum. Methods Phys. Res. Sect. B: Beam Interact. Mater. At. 374, 58–66.
59. Sabathier, C., *et al.*, 2014. In-situ TEM observation of nano-void formation in UO_2 under irradiation. Nucl. Instrum. Methods Phys. Res. Sect. B: Beam Interact. Mater. At. 326, 247–250.
60. Onofri, C., *et al.*, 2016. Evolution of extended defects in polycrystalline UO_2 under heavy ion irradiation: Combined TEM, XRD and Raman study. Nucl. Instrum. Methods Phys. Res. Sect. B: Beam Interact. Mater. At. 374, 51–57.
61. Delafoy, C., 2019. Plutonium recycling through LWR MOX fuel today and tomorrow. In: Proceedings of the International Conference on the Management of Spent Fuel from Nuclear Power Reactors 2019: Learning from the Past, Enabling the Future. IAEA, Vienna.
62. Kleykamp, H., *et al.*, 1985. Composition and structure of fission product precipitates in irradiated oxide fuels: Correlation with phase studies in the Mo-Ru-Rh-Pd and BaO-UO_2-ZrO_2-MoO_2 Systems. J. Nucl. Mater. 130, 426–433.
63. Parrish, R., Aitkaliyeva, A., 2018. A review of microstructural features in fast reactor mixed oxide fuels. J. Nucl. Mater. 510, 644–660.
64. Ronchi, C., *et al.*, 2004. J. Nucl. Mater. 327, 58–76.
65. Staicu, D., *et al.*, 2014. Effect of burn-up on the thermal conductivity of uranium–gadolinium dioxide up to 100 GWd/tHM. J. Nucl. Mater. 453 (1), 259–268.
66. Ewing, R.C., 1994. The metamict state: 1993 – The centennial. Nucl. Instrum. Methods Phys. Res. Sect. B: Beam Interact. Mater. At. 91 (1), 22–29.
67. Barney, W.K., Wemple, B.D., 1958. Metallography of UO_2-Containing Fuel Elements. Technical Report KAPL-1836. Schenectady, New York: Knolls Atomic Power Laboratory.
68. Matzke, J., 1992. On the rim effect in high burnup UO_2 LWR fuels. J. Nucl. Mater. 189, 141.
69. Matzke, H., Turos, A., Linker, G., 1994. Polygonization of single crystals of the fluorite-type oxide UO_2 due to high dose ion implantation +. Nucl. Instrum. Methods Phys. Res. Sect. B: Beam Interact. Mater. At. 91 (1–4), 294–300.
70. Rahman, M.J., *et al.*, 2018. Primary radiation damage on displacement cascades in UO_2, ThO_2 and $(U0.5Th0.5)O_2$. Comput. Mater. Sci. 154, 508–516.
71. Sonoda, T., *et al.*, 2010. Clarification of high density electronic excitation effects on the microstructural evolution in UO_2. Nucl. Instrum. Methods B 268, 3277–3281.
72. Brucklacher, D., Dienst, J., 1972. J. Nucl. Mater. 42, 285.

73. Van Brutzel, L.D., R, , Bartel, T.J., 2015. Nuclear Fuel Deformation Phenomena. Nuclear Energy Agency of the OECD (NEA).
74. Marchetti, M., *et al.*, 2017. Physical and mechanical characterization of irradiated uranium dioxide with a broad burnup range and different dopants using acoustic microscopy. J. Nucl. Mater. 494, 322–329.
75. Terrani, K.A., *et al.*, 2018. Young's modulus evaluation of high burnup structure in UO_2 with nanometer resolution. J. Nucl. Mater. 508, 33–39.
76. Klein, D., Baer, W., Smith, G.G., 1958. Nucl. Sci. Eng. 3, 698.
77. Lozano, N., *et al.*, 1998. J. Nucl. Mater. 257, 78–87.
78. Wiss, T., *et al.*, 2017. Properties of the high burnup structure in nuclear light water reactor fuel. Radiochim. Acta.
79. Matzke, H., *et al.*, 1989. J. Nucl. Mater. 166, 165.
80. Une, K., *et al.*, 1992. J. Nucl. Mater. 188, 65.
81. Une, K., *et al.*, 2001. J. Nucl. Mater. 288, 20–28.
82. Ray, I.L.F., *et al.*, 1997. J. Nucl. Mater. 245, 115–123.
83. Hiernaut, J.P., *et al.*, 2008. Fission product release and microstructure changes during laboratory annealing of a very high burn-up fuel specimen. J. Nucl. Mater. 377 (2), 313–324.
84. Rondinella, V.V., Wiss, T., 2010. The high burn-up structure in nuclear fuel. Mater. Today 13, 24–32.
85. Nogita, K., Une, K., 1994. Nucl. Instrum. Methods B B91, 301.
86. Nogita, K., Une, K., 1995. J. Nucl. Mater. 226, 302.
87. Spino, J., *et al.*, 1998. High burn-up rim structure: Evidences that xenon-depletion, pore formation and grain subdivision start at different local burn-ups. J. Nucl. Mater. 256 (2–3), 189–196.
88. Kinoshita, M., *et al.*, 2004. High Burnup Rim Project: (iii) properties of rim-structured fuel. In: 2004 International Meeting on LWR Fuel Performance. ANS: Orlando, Fl.
89. Sonoda, T., *et al.*, 2002. Transmission electron microscopy observation on irradiation-induced microstructural evolution in high burn-up UO_2 disk fuel. Nucl. Instrum. Methods Phys. Res. Sect. B: Beam Interact. Mater. At. 191 (1–4), 622–628.
90. Gerczak, T.J., *et al.*, 2018. Restructuring in high burnup UO_2 studied using modern electron microscopy. J. Nucl. Mater. 509, 245–259.
91. Miao, Y., *et al.*, 2018. Nano-crystallization induced by high-energy heavy ion irradiation in UO_2. Scr. Mater. 155, 169–174.
92. Manzel, R., Walker, C.T., 2002. EPMA and SEM of fuel samples from PWR rods with an average burn-up of around 100 MWd/kgHM. J. Nucl. Mater. 301 (2–3), 170–182.
93. Noirot, J., *et al.*, 2009. High burnup changes in UO_2 fuels irradiated up to 83 GWD/T IN M5® Claddings. Nucl. Eng. Technol. 41 (2), 155–162.
94. Noirot, J., Zacharie-Aubrun, I., Blay, T., 2018. Focused ion beam–scanning electron microscope examination of high burn-up UO_2 in the center of a pellet. Nucl. Eng. Technol 50 (2), 259–267.
95. Noirot, J., Desgranges, L., Lamontagne, J., 2008. Detailed characterisations of high burn-up structures in oxide fuels. J. Nucl. Mater. 372 (2–3), 318–339.
96. Rest, J., *et al.*, 2019. Fission gas release from UO_2 nuclear fuel: A review. J. Nucl. Mater. 513, 310–345.
97. Jegou, C., *et al.*, 2015. Raman micro-spectroscopy of UOX and MOX spent nuclear fuel characterization and oxidation resistance of the high burn-up structure. J. Nucl. Mater. 458, 343–349.
98. Rondinella, V.V., Wiss, T., 2010. The high burn-up structure in nuclear fuel. Mater. Today 13 (12), 24–32.
99. Ronchi, C., *et al.*, 1999. Thermal conductivity of uranium dioxide up to 2900K from simultaneous measurement of the heat capacity and thermal diffusivity. J. Appl. Phys. 85 (2), 776–789.
100. de Coninck, R., Devreese, J., 1969. The thermoelectric power and the conduction mechanism in nearly stoichiometric uranium dioxide single crystals. Physica Status Solidi (b) 32 (2), 823–829.
101. Desgranges, L., 2008. Is Uranium Dioxide a Glass Athigh Temperature: The Reason for Its Irradiation Resistance? Montpellier: ATALANTE.
102. Pavlov, T.R., *et al.*, 2017. Measurement and interpretation of the thermo-physical properties of UO_2 at high temperatures: The viral effect of oxygen defects. Acta Materialia 139, 138–154.
103. Szenes, G., 2005. Ion-induced amorphization in ceramic materials. J. Nucl. Mater. 336 (1), 81–89.
104. Szenes, G., 1995. General features of latent track formation in magnetic insulators irradiated with swift heavy ions. Physical Review B 51 (13), 8026–8029.
105. Baldinozzi, G., Desgranges, L., Petot, C., 2014. A statistical approach of the thermodynamic properties of UO_2 at high temperature. Nucl. Instrum. Methods Phys. Res. Sect. B: Beam Interact. Mater. At. 327, 68–73.
106. Ruello, P., *et al.*, 2005. Heat capacity anomaly in UO_2 in the vicinity of 1300K: An improved description based on high resolution X-ray and neutron powder diffraction studies. J. Phys. Chem. Solids 66 (5), 823–831.
107. Konings, R.J.M., Beneš, O., 2013. The heat capacity of NpO_2 at high temperatures: The effect of oxygen Frenkel pair formation. J. Phys. Chem. Solids 74 (5), 653–655.
108. Desgranges, L., *et al.*, 2012. How polarons can enhance UO_2 irradiation resistance? Nucl. Instrum. Methods Phys. Res. Sect. B: Beam Interact. Mater. At. 277, 109–111.
109. Youinou, G., Vasile, A., 2005. Plutonium multirecycling in standard PWRs loaded with evolutionary fuels. Nucl. Sci. Eng 151, 25–45.